scientific reports

Check for updates

OPEN

Identification of oncogenes associated with colorectal cancer mortality and the effect of cinnamon-conjugated magnetic nanoparticles on their expression

Mohammad Amin Ahmadzadeh Chaleshtori[1], Ali Salehzadeh[1]✉ & Maryam Peymani[2]

Finding the molecular targets involved in the severity and drug resistance of Colorectal cancer (CRC) and applying targeted treatments against them is a promising approach. In this study, some candidate oncogenes related to disease severity and mortality were identified by extracting bioinformatics data, and the effect of Fe_3O_4@Glu-Cinnamon NPs on the survival of CRC cells (SW480) and the expression of these oncogenes was investigated. The NPs were characterized by FT-IR, XRD, DLS and zeta potential measurement, TEM and SEM imaging, EDS-mapping and VSM analysis. Cytotoxicity of the NPs was evaluated by the MTT assay and a flow cytometry analysis was done to investigate cell apoptosis/necrosis levels and cell cycle analysis of cancer cells. The Fe_3O_4@Glu-Cinnamon NPs with spherical morphology were correctly synthesized, containing no elemental impurities, with a size range of 26.8–60.2 nm, DLS of 213 nm, zeta potential of -15.4mV and maximum magnetization level of 20.33emu/g. Treatment of cancer cells with the NPs elevated primary and late apoptosis and cell necrosis levels to 20.85, 16.83 and 9.56% and treated cells were mainly arrested at the S and G2/M phases. The expression level of the oncogenes associated with mortality, *SNAI1*, *THBS2* and *INHBA* reduced to 0.74, 0.66 and 0.7 folds, respectively. The magnetic properties of Fe_3O_4 NPs enable their potential use in targeted drug delivery, allowing for site-specific accumulation within tumors. This could minimize systemic toxicity while enhancing treatment efficacy.

Keywords Colorectal cancer, Cinnamon, Iron oxide nanoparticles, Oncogene

Colorectal cancer (CRC) is among the leading causes of morbidity and mortality throughout the world as it is the third most common type of diagnosed cancer with an estimated 1.88 million new cases and 915,000 deaths each year[1]. With a mortality percentage of ~ 49%, CRC is considered a major health problem, and the presentation of new diagnostic and treatment approaches to deal with this disease is one of the priorities of global health. The disease trend in high-income countries varies from region to region, declining, stabilizing, or increasing in the different areas. On the other hand, the disease has been growing in most developing and low-income countries[2].

Several contributing factors such as Genetics, lifestyle, age, ethnicity, diet, etc. are involved in the initiation and development of CRC, among which genetic factors are a main contributing determinant in the emergence of CRC. Three main molecular mechanisms have been proposed for the initiation and development of CRC, including chromosomal instability, CpG island methylator phenotype and microsatellite instability. Chromosomal instability, which initiates with mutations in the adenomatous polyposis coli, is the most commonly known triggering mechanism for CRC that leads to activation of the oncogene *KRAS* and inactivates tumor suppressor protein TP53[3]. Despite this, the subsequent molecular mechanisms involved in the development and virulence of CRC that contribute to the severity of the disease and mortality rate are less understood. Therefore, in-depth identification and characterization of the molecular mechanism of this disease and finding molecular targets for the targeted chemotherapy are among the research priorities.

Early detection and effective treatment methods are two main goals in research studies on cancer biology. Nanotechnology provides promising results in cancer detection and treatment, aiming to provide molecular imaging, drug delivery, targeted therapy, etc[4,5]. Accurate targeting of cancer tissues using nanoparticles has

[1]Department of Biology, Rasht Branch, Islamic Azad University, Rasht, Iran. [2]Department of Biology, ShK. C., Islamic Azad University, Shahrekord, Iran. ✉email: a.salehzadeh@iau.ac.ir

been associated with promising successes. Such an approach can improve the effectiveness of the treatment and minimize its side effects[6]. For this reason, the use of magnetic nanoparticles in the design of anti-cancer nanomedicines has attracted the attention of researchers. Due to their small size, nanoparticles can easily penetrate the host tissues, reach the cancerous tissues and enter the target cells[6]. Conducting magnetic nanoparticles using magnetic force provides efficient drug delivery to cancer cells. In addition to small size and magnetic properties, biocompatibility is another influential parameter in the use of nanoparticles in biomedical fields, including cancer diagnosis and treatment[7]. Despite having significant anticancer properties, many metal nanoparticles cannot have clinical applications due to their toxic properties on biological systems. Iron oxide nanoparticles can be considered among the most widely used metal nanoparticles in cancer diagnosis and treatment. Due to their magnetic properties, iron oxide nanoparticles can be used in the imaging of cancerous tumors to improve image contrast. Also, they can be considered as drug carriers for drug delivery to tumor tissues[8]. Moreover, the functionalization of iron oxide nanoparticles provides the possibility of controlled and stable drug release, which can improve the effectiveness of chemotherapy[9]. Besides, iron oxide nanoparticles are generally considered biocompatible and biodegradable, which makes them suitable for biomedical applications compared to other metal nanoparticles.

Many bioactive compounds such as flavonoids, phenolics and proteins with anticancer potential have been identified in plant species[10]. Cinnamon, a dry substance from the bark of the Cinnamomum plant, has many uses in the food industry as a flavoring and aromatic substance[11]. Previous studies have shown that this substance contains a variety of bioactive compounds such as cinnamaldehyde and eugenol, which have inhibitory properties on cancer cells[11,12]. Therefore, the bioactive compounds from cinnamaldehyde can be used for drug formulation against cancers. However, there are several limitations and challenges regarding its application in cancer treatment. Similar to many herbal bioactive compounds, the bioavailability of the bioactive compounds from cinnamon is relatively low, which means that the therapeutic molecules are not adequately absorbed by the tissues and are mainly excreted from the body[13]. Nanotechnology can be used to improve the bioavailability of such compounds. Magnetic nanoparticles can also be considered as tools for carrying and delivering such compounds to cancer tissues, a process that reduces the rapid clearance of the drug from the body and provides gradual drug release, thus improving their bioavailability and effectiveness. Studies have reported the biosafety of iron oxide nanoparticles and highlighted their potential for safe clinical application. Investigations into the long-term effects of iron oxide nanoparticles have shown that they can be effectively cleared from the body, indicating the promise of iron oxide nanoparticles as biocompatible agents in anticancer therapies[14,15].

Functionalizing magnetic nanoparticles with cinnamon may enhance their therapeutic potential by facilitating targeted delivery while simultaneously exerting intrinsic anticancer effects. The bioavailability of cinnamon-derived compounds can be improved through nanoparticle conjugation, ensuring better cellular uptake and sustained release. The conjugation of cinnamon with magnetic nanoparticles allows for magnetic targeting, ensuring that the therapeutic effects are concentrated at the tumor site, and thereby reducing systemic toxicity[16]. This study has two main objectives; the first is to identify oncogenes associated with poor prognosis and mortality in colorectal cancer, with a specific focus on the upregulated genes SNAI1, THBS2, and INHBA, which were identified through TCGA data analysis. These genes were found to be significantly upregulated in colorectal cancer samples and are linked to critical malignancy pathways such as metastasis, angiogenesis, hypoxia, and inflammation. The second aim is to evaluate the effect of magnetic iron oxide nanoparticles conjugated with cinnamon extract on the expression of these genes in colorectal cancer cell lines.

Materials and methods

Data sources

The flowchart presented in Fig. 1 illustrates the overall steps of the study. To identify genes whose expression changes might be associated with colorectal cancer malignancy, transcriptomic data from colon cancer (TCGA-COAD) were utilized (https://portal.gdc.cancer.gov/projects/TCGA-COAD). Initially, raw data from this cancer type were downloaded using the TCGAbiolinks package (https://bioconductor.org/packages/release/bioc/html/TCGAbiolinks.html). Subsequently, genes with zero or near-zero expression, based on the CPM (Count per Million) criteria, where CPM was less than 10 in 70% of samples, were removed from the expression matrix using the edgeR package (https://bioconductor.org/packages/release/bioc/html/edgeR.html). Next, data normalization was performed using the TMM (Trimmed Mean of M values) method and the data were log-transformed to base 2. The resulting expression matrix was used for all analyses, including differential expression between groups and the investigation of the relationship between gene expression and patient prognosis. The TCGA data for colorectal cancer included 480 tumor samples at various stages and 41 normal samples. Additionally, the latest clinical data updates for TCGA-COAD were downloaded and incorporated into the analysis. For further validation, data from the GEO database were used, and raw microarray data with the accession number GSE39582 were downloaded. This study comprised 566 colorectal tumor samples and 19 normal colon samples. Initial preprocessing of these data included background correction, normalization based on the RMA method, and log2 transformation of the data using the limma package. Finally, the resulting expression matrix was used to examine differential gene expression.

Preprocessing of clinical and prognostic data

The clinical data from TCGA-COAD were used to investigate the correlation between the expression of candidate genes and patient mortality rates in colorectal cancer. Initial preprocessing of the clinical data involved excluding samples with survival days recorded as 0, 1, or NA. Additionally, for deceased samples, only those were considered where the death was due to the presence of a tumor and cancer was the cause of death. To examine the relationship between the expression of candidate genes and patient mortality rates, the expression levels of all candidate genes for the samples meeting the specified clinical criteria were first extracted. Then, the expression

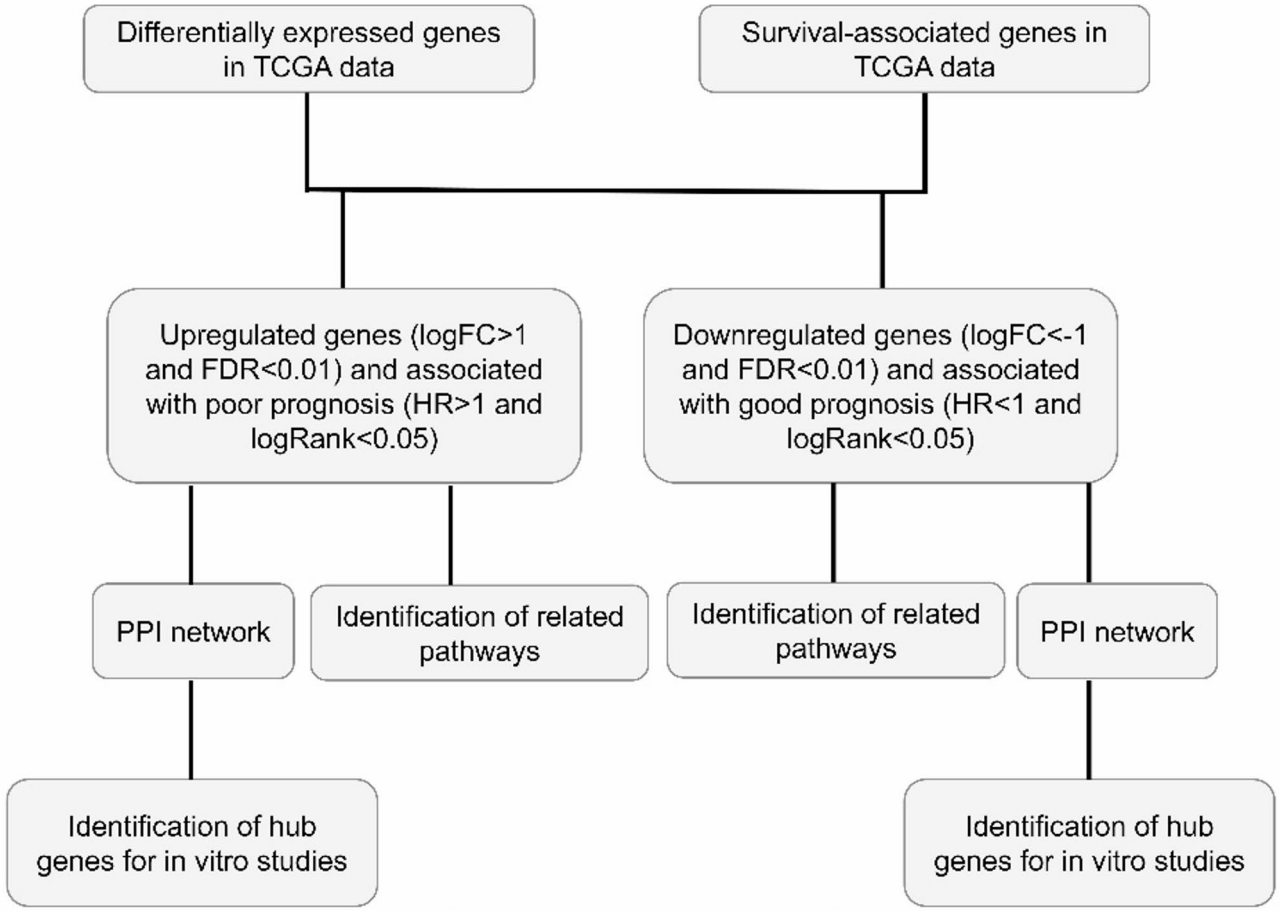

Fig. 1. The flowchart that illustrates the overall steps of the study.

of each candidate gene across all samples was standardized to a Z-score. The univariate Cox regression test was used to assess the association between the expression of the candidate genes and patient prognosis. To further validate the results, Kaplan-Meier (K-M) curves were employed. For this analysis, the cancer samples were divided into two groups—High and Low—based on the median expression of the candidate genes, and the relationship between gene expression levels and patient mortality rates was examined using the K-M curves.

Databases

To identify pathways associated with candidate genes, the Enrichr database (https://maayanlab.cloud/Enrichr/) and the MSigDB repository were utilized. Additionally, for constructing protein-protein interaction (PPI) networks, the STRING database (https://string-db.org/) was employed.

Synthesis of nanoparticles

Synthesis of iron oxide (Fe_3O_4) nanoparticles (NPs) was performed according to the method described by Mahdavi Niyaki et al. (2024) with minor modifications[17]. In brief, 3.2 g of $FeCl_2.4H_2O$ and 7.6 g of $FeCl_3.6H_2O$ were dissolved in deionized water and maintained at 85 °C for 60 min. Next, NH_3 solution was added and the solution was kept at 85 °C and low flow N_2 was applied until the formation of Fe_3O_4 NPs. The synthesized NPs were collected and dried and then, subjected to functionalization with D- glucose. To functionalize the NPs, at first one gram of the synthesized NPs and 500 mg of D-glucose were dissolved in deionized water, and sonication was applied for 30 min to disperse the particles. Next, the mixture was heated at 180 °C for 3 h. Finally, the functionalized NPs were collected and dried at 65 °C. At the final step, the NPs were conjugated to cinnamon extract (Sigma-Aldrich, reagent grade: ≥ 95%,). In brief, one gram of the functionalized NPs and 100 µL of cinnamon were dissolved in distilled water and the mixture was shaken overnight. Then, the Fe_3O_4@Glu-Cinnamon NPs were collected, washed with distilled water and dried at 65 °C.

Physicochemical properties of the NPs

A Perkin-Elmer spectrum 100 FT-IR instrument was employed to determine the functional groups of the synthesized nanoparticles and cinnamon in an absorption wavelength range between 500 and 4000 cm^{-1}. The crystal structure of the Fe_3O_4@Glu-Cinnamon NPs was investigated using an XRD device (Philips PW1730, (Cu-Kα X-ray tube, $\lambda = 1.54056$ A) and at 2θ from 10 to 80 degrees. Electron microscopy was done using SEM (TESCAN Mira3) and TEM (Zeiss EM900) microscopes to determine the morphological features of the NPs.

The elemental composition of the NPs was determined using Energy-Dispersive X-ray spectroscopy (EDS) (TESCAN Mira3). The DLS and zeta potential measurement analysis was also done by a HORIBA Scientific SZ-100 zeta sizer. The magnetic properties of Fe_3O_4@Glu-Cinnamon NPs were investigated using a VSM device (Meghnatis Daghigh Kavir company, LBKFB).

Cell lines and cell survival assay

The studied cell lines, including a colorectal cancer cell line (SW480) and a normal human cell line (HEK293), were received from the Pasteur Institute of Iran. The cells were cultured in Dulbecco's modified Eagle medium (DMEM) in 25 cm^2 cell culture flasks and after reaching confluency of 80%, the cells were harvested, their density was adjusted to 1×10^5 cell/mL and used for the cell viability assay. To perform the assay, at first, 100 µL of cell suspension was added to the wells of a 96-well cell culture plate and then, treated with different concentrations of cinnamon and Fe_3O_4@Glu-Cinnamon NPs (0, 31.25, 62.5, 125, 250, 500 and 1000 µg/mL). The cells were incubated for 24 h after which their survival level was quantified using the MTT (2-(4,5-dimethythiazol-2-yl) -2,5-diphenyltetrazolium bromide), according to the method described by Esfahani et al.[18]. In brief, 200 µL of 0.5 mg/mL MTT solution was added to the wells and incubated for 4 h. Then, the medium was removed and 200 µL of DMSO was added and kept at 25 °C for 30 min with shaking at 100 rpm. Finally, the OD at 570 nm was measured and the effect of cinnamon and Fe_3O_4@Glu-Cinnamon NPs on the cell viability was calculated as follows[19]:

$$Inhibition\ percentage = \frac{OD570\ of\ untreated\ wells - OD570\ of\ treated\ wells}{OD570\ of\ untreated\ wells} \times 100$$

Flow cytometry

Flow cytometry assay was used to evaluate to quantify the population of apoptotic, necrotic and healthy cells in nanoparticle-treated and control groups. At first, the colorectal cancer cells were treated with an IC_{50} concentration of the Fe_3O_4@Glu-Cinnamon NPs for 24 h. Then, the cells were subjected to staining with propidium iodide (PI) and Annexin V (BioLegend, USA). Next, the frequency of cell apoptosis and necrosis was quantified by a flow cytometry device (ZE5, Bio-Rad, USA).

A Flow cytometry analysis was also performed to analyze the cell cycle phases of the treated and control CRC cells. After a 24-hour treatment, the cell culture medium was aspirated, 200 µL of cold ethanol was added, and after evaporation of ethanol, the cells were stained with PI and RNase A. Finally, the DNA content of the cells, which is an indicator of the cell cycle phases, was quantified by a flow cytometry device.

Hoechst staining

To investigate the possible nuclear damage in SW480 cells due to exposure to Fe_3O_4@Glu-Cinnamon NPs, the cells were treated with an IC_{50} concentration of the NPs for 24 h. Next cell staining was done with Hoechst dye for 10 min. Next, the cells were examined under a fluorescent microscope and compared with untreated stained cells[20].

Real-time PCR

Based on the bioinformatics investigation, that was described above, the effects of the Fe_3O_4@Glu-Cinnamon NPs on the expression level of the oncogenes *SNAI1*, *THBS2* and *INHBA* was investigated using a real-time PCR assay. The cells were treated with the NPs for 24 h, after which their RNA content was extracted using a BioLegend commercial kit and cDNA was prepared using the SinaClone kit (Iran). The fragments were amplified using specific primers (Table 1), which were designed using the Gene Runner software (version 6) (https://gene-runner.software.informer.com/6.0/) and SYBR-Green real-time PCR assay kit (Denazist, Iran) in an ABI 7500 thermocycler device. The *GAPDH* gene was used as the housekeeping gene to normalize the real-time PCR data and the relative expression levels of the genes were calculated using the $2^{-\Delta\Delta CT}$ method, as described by Pfaffl et al.[21].

Statistical analysis and software

All initial preprocessing of the raw data from TCGA and GEO was conducted using the R programming language (version 4.0.2), leveraging the latest updates of the aforementioned packages. To analyze differential expression between groups, the linear model approach was used, and the significance level was determined using the False Discovery Rate (FDR) test. For assessing the significance of survival-related analyses, the log-rank test was applied. All figures and charts were generated using GraphPad Prism software (version 8). The

Gene	Sequence (5–3′)		Product length (bp)
	Forward	Reverse	
SNAI1	TAGCGAGTGGTTCTTCTGCG	AGGGCTGCTGGAAGGTAAAC	164
THSB	CTCGGTCCGGAACACTGAAA	CACAGAGCCAGCAGGACC	106
INHBA	GCTCAGACAGCTCTTACCACA	AAAAGGCCCTGCTTTTCCTCC	172
GAPDH	CCCACTCCTCCACCTTTGAC	CATACCAGGAAATGAGCTTGACAA	75

Table 1. Sequence of the primers that were used in this work.

experimental assays were done in triplicates and one-way ANOVA was used to evaluate significant differences between treatment groups and p-values of less than 0.05 was considered as statistically significant.

Results

Expression changes of multiple genes in colorectal cancer and their association with patient mortality rates

To identify genes whose expression changes might be associated with the malignancy of colorectal cancer, TCGA data were utilized. Differential expression analysis revealed that a total of 1,052 genes were significantly upregulated in cancer samples compared to normal ones, with criteria of logFC > 1 and FDR < 0.01 (Fig. 2). Furthermore, 2,107 genes showed significant downregulation with criteria of logFC < -1 and FDR < 0.01 (Fig. 3). The relation between the expression of these identified genes and patient survival rates was also examined. Cox regression analysis indicated that upregulation of 1,726 genes was significantly associated with poor prognosis (HR > 1 and log-rank < 0.05) (Fig. 3A). The overlap between the 1,052 upregulated genes and the 1,726 genes linked to poor prognosis revealed that 53 genes exhibited both characteristics (Fig. 3B). Conversely, 738 genes were found to have increased expression associated with a good prognosis (Fig. 3A). The overlap analysis of

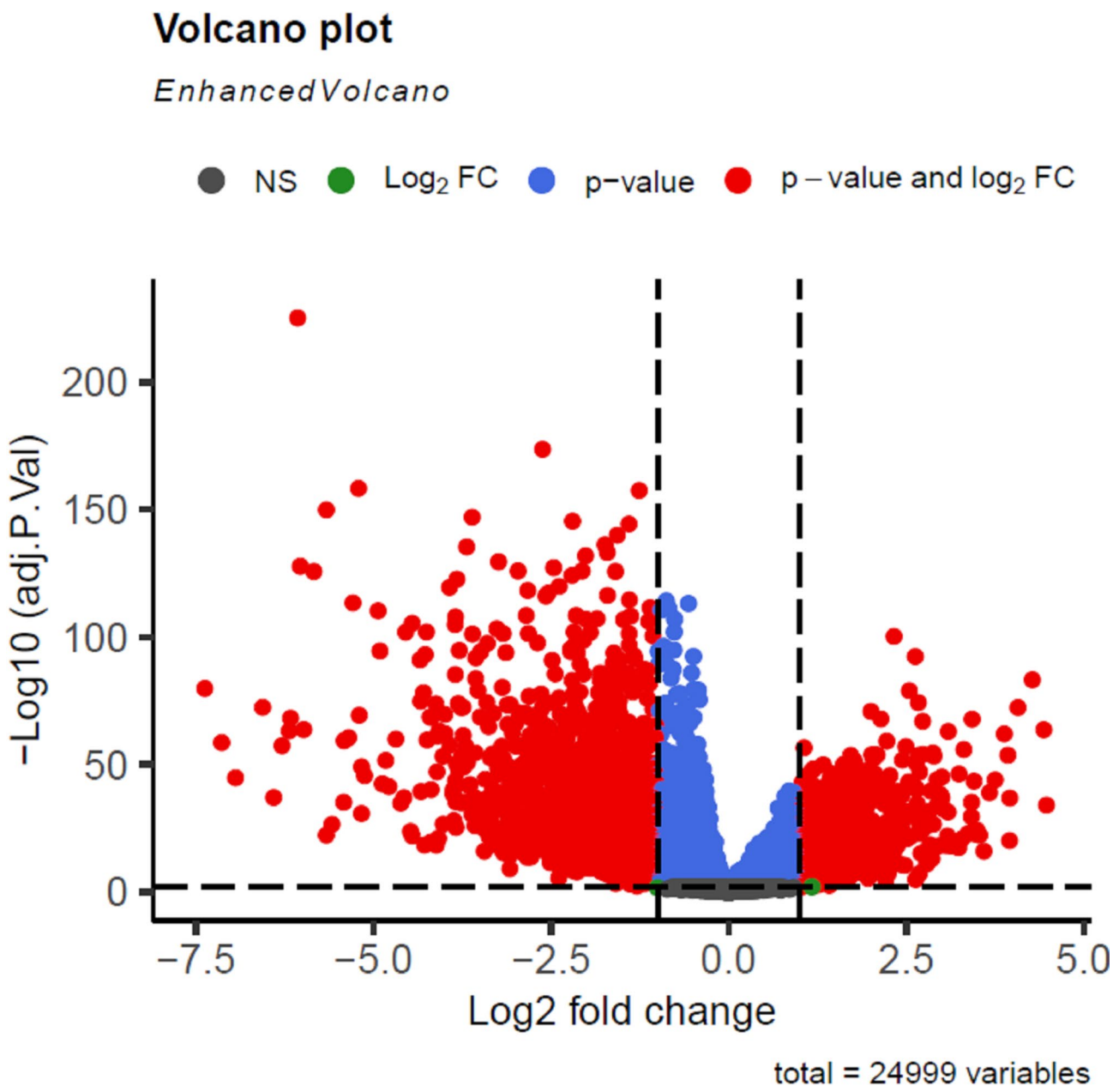

Fig. 2. Differential expression analysis of multiple genes in Colorectal Cancer. The results revealed that a total of 1052 genes were significantly upregulated in cancer samples compared to normal ones and 2107 genes showed significant downregulation.

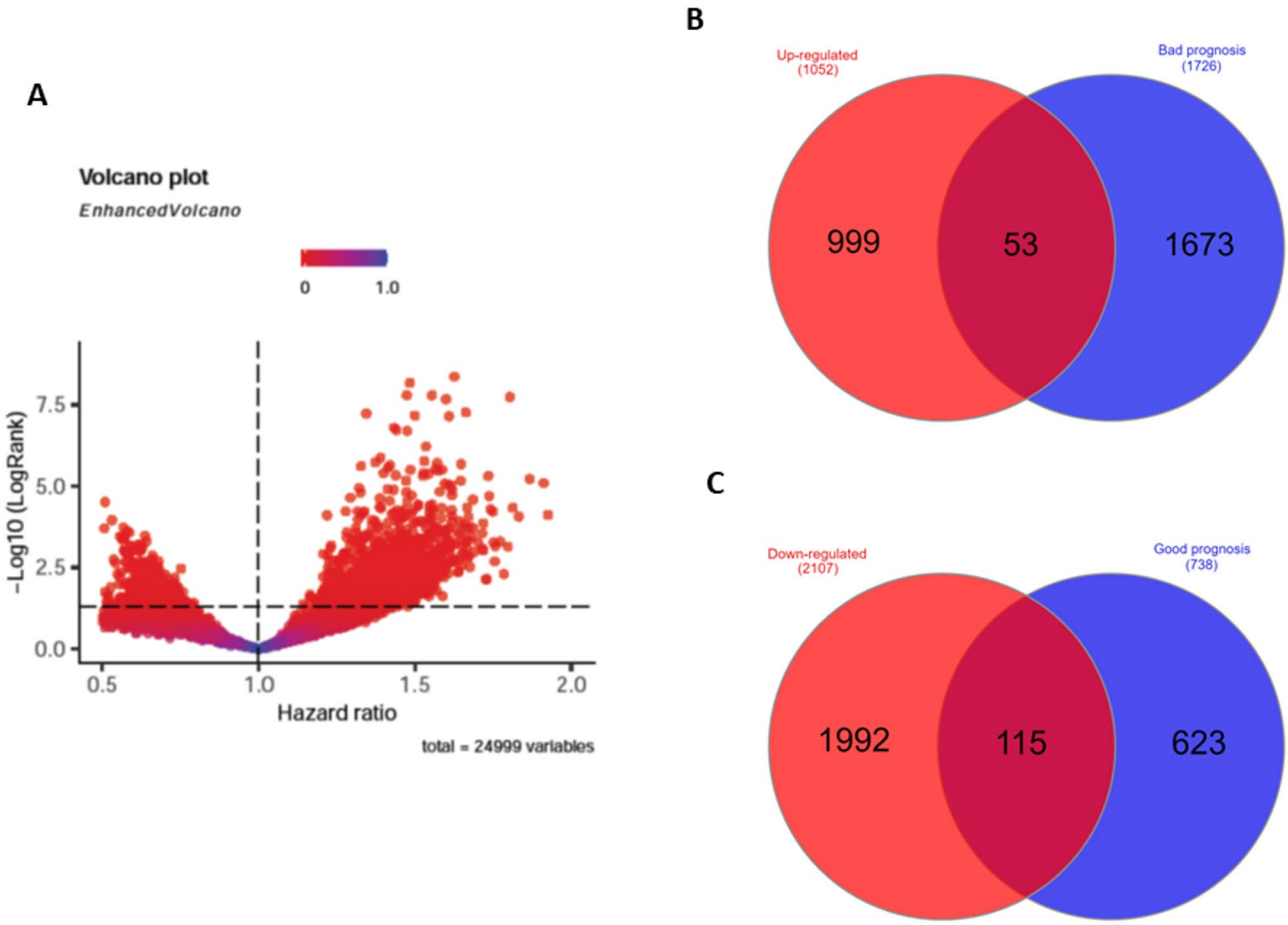

Fig. 3. Relation between the expression of the identified genes and patient survival rates. A total number of 53 genes were identified as having both significant upregulation and association with poor prognosis, while 115 genes were downregulated and associated with a good prognosis.

downregulated genes and those associated with a good prognosis identified 115 genes with both attributes (Fig. 3C). Ultimately, 53 genes were identified as having both significant upregulation and association with poor prognosis, while 115 genes were downregulated and associated with a good prognosis. These genes were selected for further analysis. These findings suggest that the identified candidate genes might play a role in the pathogenesis of colorectal cancer.

Association of candidate genes with malignancy pathways

To gain further insights into the candidate genes, their associated pathways were investigated. Enrichment analysis of the 53 upregulated genes indicated that many of them are involved in cellular processes such as metastasis, angiogenesis, hypoxia, and inflammation (Fig. 4A). Conversely, the enrichment analysis for the 115 downregulated genes associated with a good prognosis suggested that some are involved in pathways like fatty acid metabolism, propanoate metabolism, and the citrate cycle (Fig. 4B). These results suggest that the candidate genes are linked to pathways associated with malignancy, such as metastasis and metabolic alterations. Using the PPI network, hub genes were identified. For the 53 upregulated genes associated with poor prognosis, 18 genes were found to be interconnected (Fig. 5). PPI network analysis revealed that among these, *SERPINE1*, *SPP1*, *SNAI1*, *THBS2*, and *INHBA1* had the highest degree of interaction (degree > 7) and could be considered hub genes for this group (supplementary file). Conversely, for the 115 downregulated genes associated with a good prognosis, 36 genes were identified as interconnected (Fig. 6). PPI network analysis showed that *ACOX1*, *ACO2*, *ACSS2*, *PPARGC1A*, and *CLCA1* had the most interactions with other genes (supplementary file). These findings indicate that these genes might play crucial roles in the pathogenesis of colorectal cancer.

Physicochemical properties

The FT-IR analysis of Fe_3O_4 indicated sharp absorption peaks at 420 and 580 cm^{-1} that are due to the Fe-O bond related to the Fe^{2+} and Fe^{3+} ions located at the octagonal phase and Fe^{3+} at the tetragonal phase that indicate the formation of the Fe_3O_4 structure[22]. The FT-IR of cinnamon exhibited absorption peaks at 557, 799 and 896 cm^{-1} that belong to the C-C, C-H and =CH bonds, respectively. The peak at 1385 cm^{-1} is related to the C-C bond of the benzene ring of the cinnamon. The peaks at 1608, 1743 and 3431 cm^{-1} are associated with the C=O,

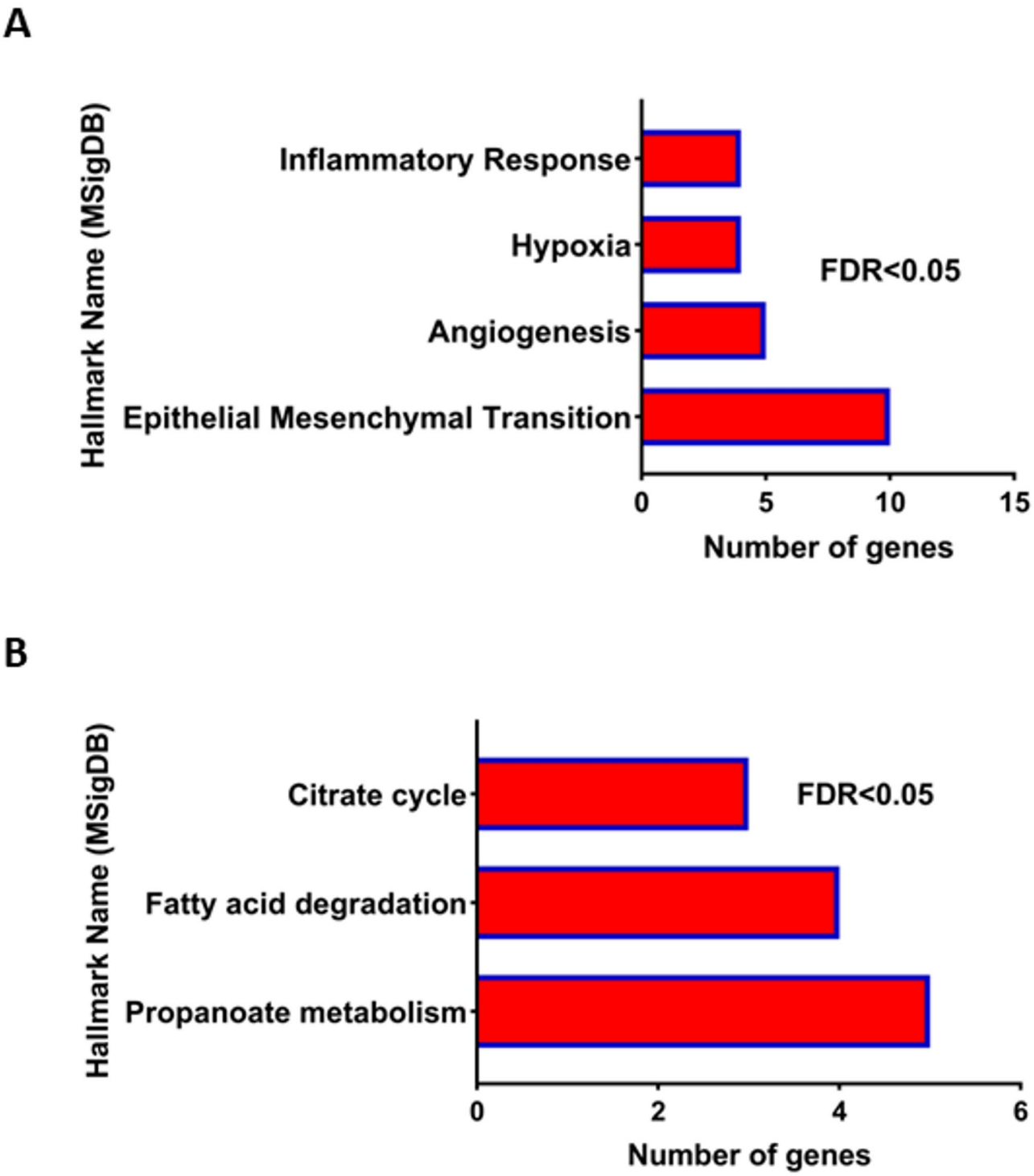

Fig. 4. Association of candidate genes with malignancy pathways. Enrichment analysis of the 53 upregulated genes indicated that many of them are involved in cellular processes such as metastasis, angiogenesis, hypoxia, and inflammation (**A**) and the 115 downregulated genes associated with a good prognosis suggested that some are involved in pathways like fatty acid metabolism, propanoate metabolism, and the citrate cycle (**B**).

C = C and –OH bonds of cinnamon. The spectrum c that displays the FT-IR pattern of Fe_3O_4@Glu-Cinnamon NPs shows a peak at 712 cm^{-1}, related to the presence of Iron oxide, and several peaks at 1165, 1460. 1616 and 1746 indicate the presence of C-O, C-C, C = C and C = O bonds. The peaks at 2853, 2937 and 3435 indicate the presence of an O-H bond. Considering the presence of peaks related to Fe_3O_4 and cinnamon in the structure of the composite, it can be concluded that the composite has been correctly synthesized (Fig. 7).

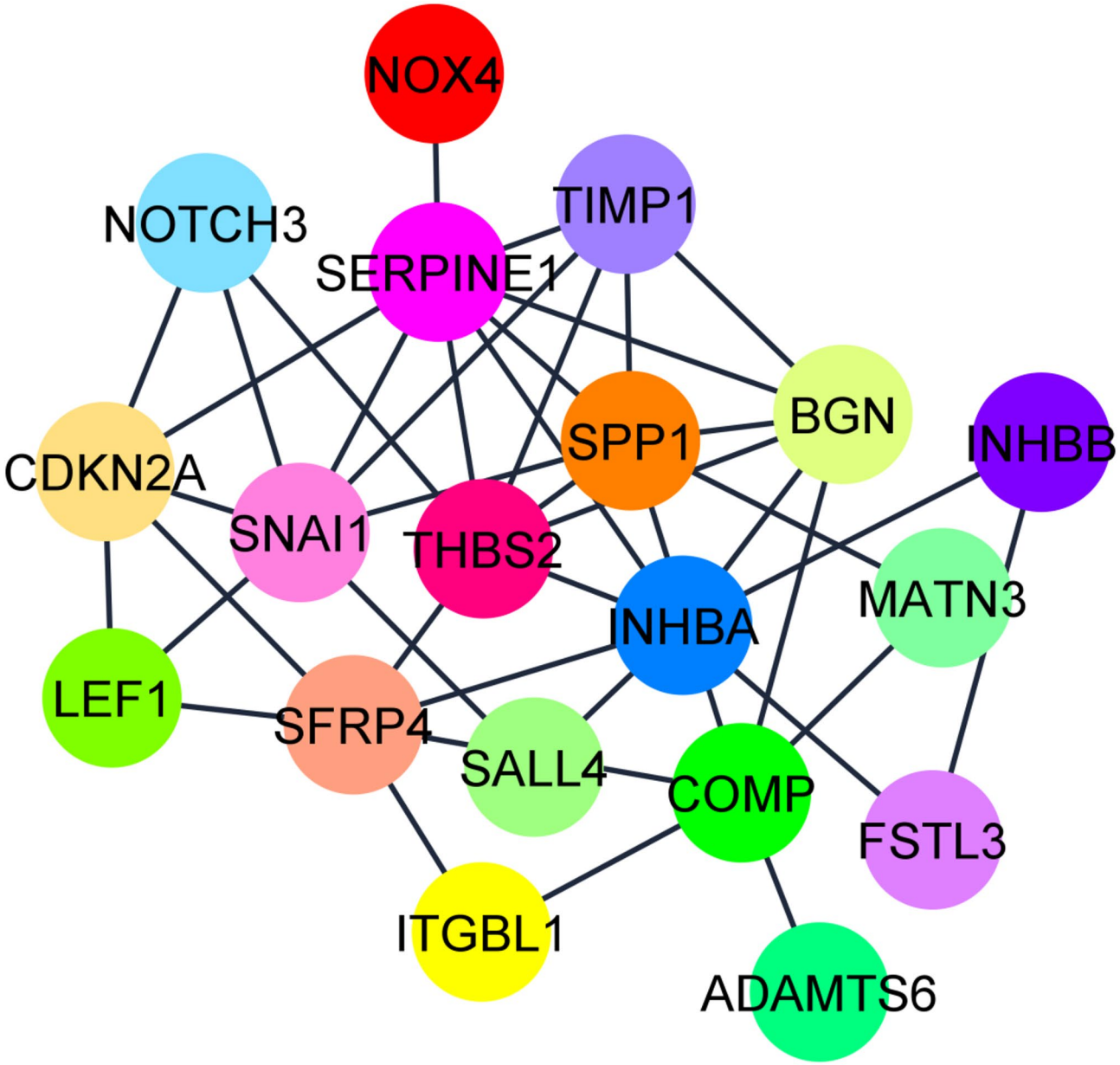

Fig. 5. Identification of hub genes using the PPI network for the upregulated genes. For the 53 upregulated genes associated with poor prognosis, 18 genes were found to be interconnected, among which the *SERPINE1*, *SPP1*, *SNAI1*, *THBS2*, and *INHBA* had the highest degree of interaction (degree > 7).

The peaks at 2θ of 33.06, 35.61, 54.07 and 62.81 in the XRD spectrum of Fe_3O_4@Glu-Cinnamon NPs indicate the presence of the Iron oxide NPs and comply with the JCPDS card Number 03-0863[18,23]. The peaks at 2θ of 30.12 may be due to the presence of D-glucose[24]. Also, due to the amorphous structure of cinnamon, Sharpie peaks can be seen at 2θ between 10 and 20° in this spectrum (Fig. 8). According to the electron microscopy images, the Fe_3O_4@Glu-Cinnamon NPs were almost spherical and their size ranged from 26.8 to 60.2 nm (Fig. 9a and b). In addition, the elemental composition of the NPs includes Fe (43.3 w%), C (35.2 w%) and O (21.6 w%) atoms that indicate the purity of the NPs (Fig. 9c). The DLS and zeta potential measurement analyses showed that the particle size in an aqueous medium was 213 nm and their surface charge was − 15.4 mV (Fig. 10a and b). Investigation of the magnetic properties of the Fe_3O_4@Glu-Cinnamon NPs by VSM analysis showed that the maximum magnetization level of the NPs was 20.33 emu/g, which was observed at an applied field of 14,000 Oe (Fig. 11).

Cell survival assay

Cell viability analysis, performed on the normal human cells, showed that Fe_3O_4@Glu-Cinnamon NPs significantly reduced cell viability levels at all studied concentrations. The IC_{50} value of Fe_3O_4@Glu-Cinnamon NPs for the normal cell line (HEK293) was 340 µg/mL. The IC_{50} value of Fe_3O_4@Glu-Cinnamon NPs on the

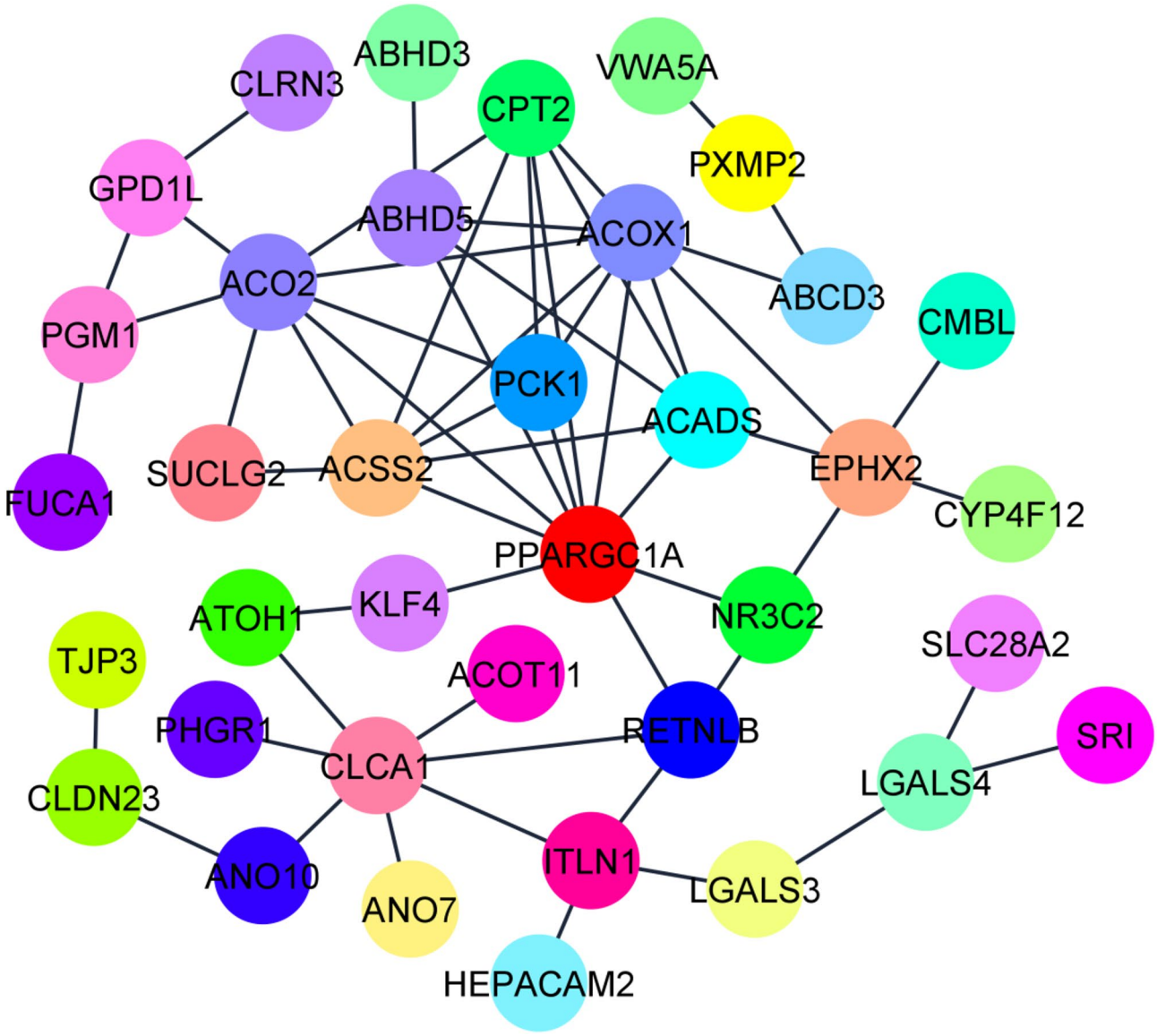

Fig. 6. Identification of hub genes using the PPI network for the downregulated genes. For the 115 downregulated genes associated with a good prognosis, 36 genes were identified as interconnected. The *PXMP2*, *ACOX1*, *ACO2*, *ACSS2*, *PPARGC1A*, and *CLCA1* had the most interactions with other genes.

cancer cell line (SW480) was 127 µg/mL and the IC_{50} value of cinnamon alone on cancer the cell line was 362 µg/mL (Fig. 12).

Flow cytometry

Investigation of the effect of Fe_3O_4@Glu-Cinnamon NPs on the cell apoptosis/necrosis levels showed that the nanoparticles cause a considerable increase in the apoptosis and necrosis levels in the colorectal cancer cell line. The percentage of primary and late apoptosis in the untreated cells were 0.03 and 0.01%, respectively, but increased to 20.85 and 16.83% following the exposure to Fe_3O_4@Glu-Cinnamon NPs. In addition, the percentage of cell necrosis elevated from 3.98% in the control cells to 9.56% in the treated group. The results are presented in Fig. 13.

Cell cycle analysis of the control SW480 cell line showed that 62.7, 21.90 and 14.2% of the cells were at the G0/G1, S and G2/M phases, respectively. In contrast, after treatment of the cells with Fe_3O_4@Glu-Cinnamon NPs, the frequency of the cells at the G0/G1 phase reduced to 50.3% and 32.0% of the cells were at the S phase. In addition, a slight increase in the frequency of the cells at the G2/M phase was observed (16.1%) (Fig. 14).

Nuclear damage

Hoechst staining of the SW480 cells showed that the exposure to Fe_3O_4@Glu-Cinnamon NPs causes severe nuclear damage such as chromatin condensation and fragmentation. In addition, apoptotic bodies were observed in the treated cells. Figure 15 displays Hoechst staining of the SW480 cells.

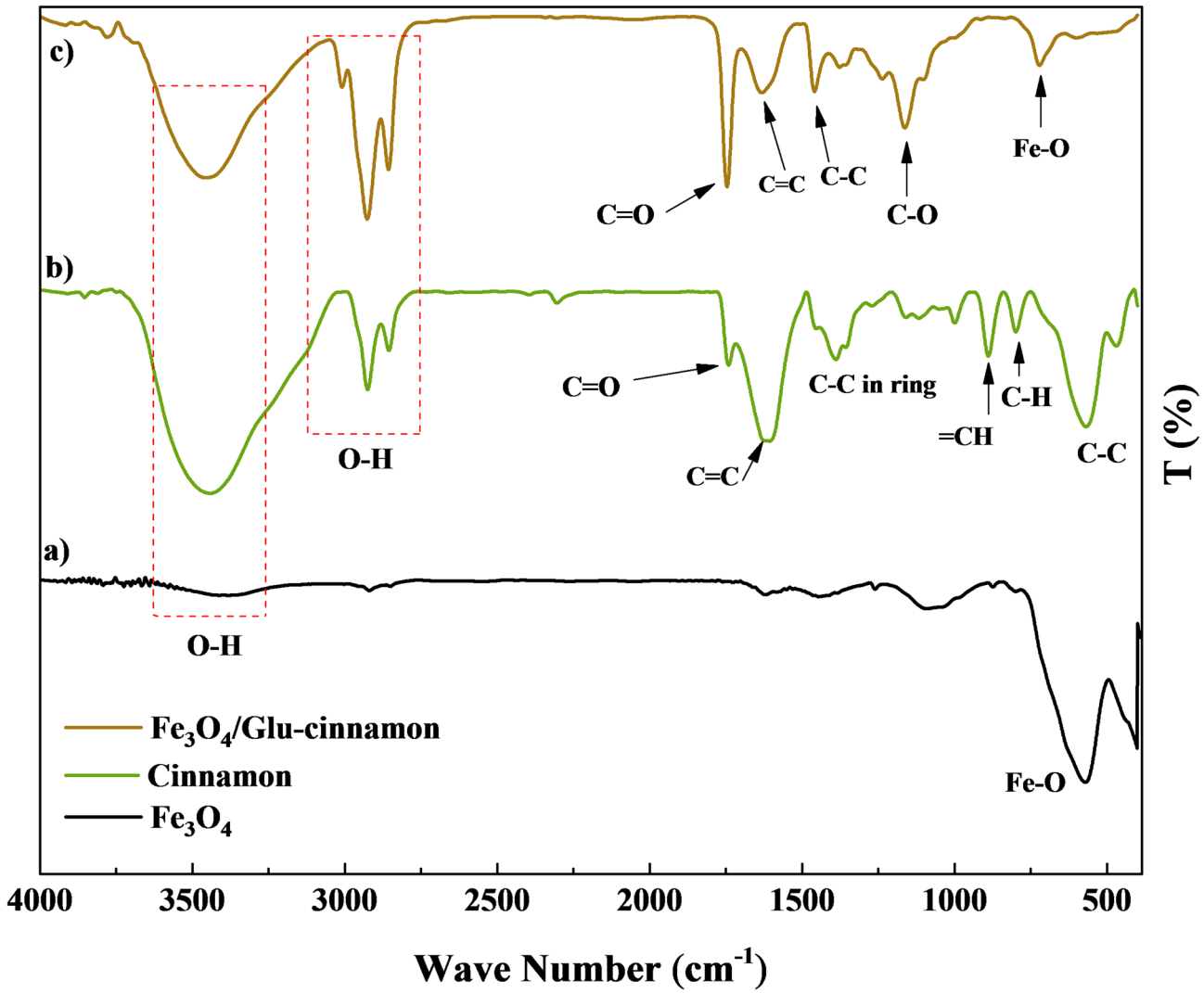

Fig. 7. FT-IR of Fe_3O_4 NPs (**a**), Cinnamon (**b**) and Fe_3O_4@Glu-Cinnamon NPs (**c**).

Gene expression

Real-time PCR was employed to quantify the expression levels of the *SNAI1*, *THBS2* and *INHBA*, the oncogenes associated with mortality in colorectal cancer. We found that the treatment of the SW480 cells with Fe_3O_4@Glu-Cinnamon NPs causes a significant reduction in the expression levels of all studied oncogenes. The expression level of the *SNAI1* was reduced to 0.74 folds, and *INHBA* was downregulated to 0.70 folds. In addition, a significant reduction was observed in the expression level of the *THBS2* oncogene (0.66 folds). The results are displayed in Fig. 16.

Discussion

Colorectal cancer is a frequent disease and among a leading cause of mortality in cancer cases. An increasing trend in the mortality of colorectal cancer in many parts of the world has been observed. This increasing trend is associated with several factors such as changes in lifestyle and human diet, as well as late diagnosis and inefficient treatment[25]. Current treatment interventions include surgical removal of tumor tissues and adjuvant chemotherapy, which are unsuccessful in treating the disease in many cases. Targeted treatment of tumor tissues not only can reduce the side effects of treatment but also can improve the effectiveness of chemotherapy[26]. Magnetic nanoparticles have received attention in cancer chemotherapy as they are small enough to penetrate body tissues and can be delivered to the tumor tissues using a magnetic force. This approach provides the possibility of more effective drug delivery to the target tissues, which leads to more effective treatment. In this study, initially, the candidate oncogenes associated with mortality in CRC were identified using bioinformatic tools, then, the effects of Fe_3O_4@Glu-Cinnamon NPs on the viability of the colorectal cancer cells and expression of the selected candidate genes were characterized.

Several factors such as the quality of precursor material and variation of reaction conditions such as temperature and stirring speed can affect the physicochemical and biological properties of the synthesized nanoparticles. Standardizing the synthesis protocol can help consistency and reduce Batch-to-batch variability in the synthesis

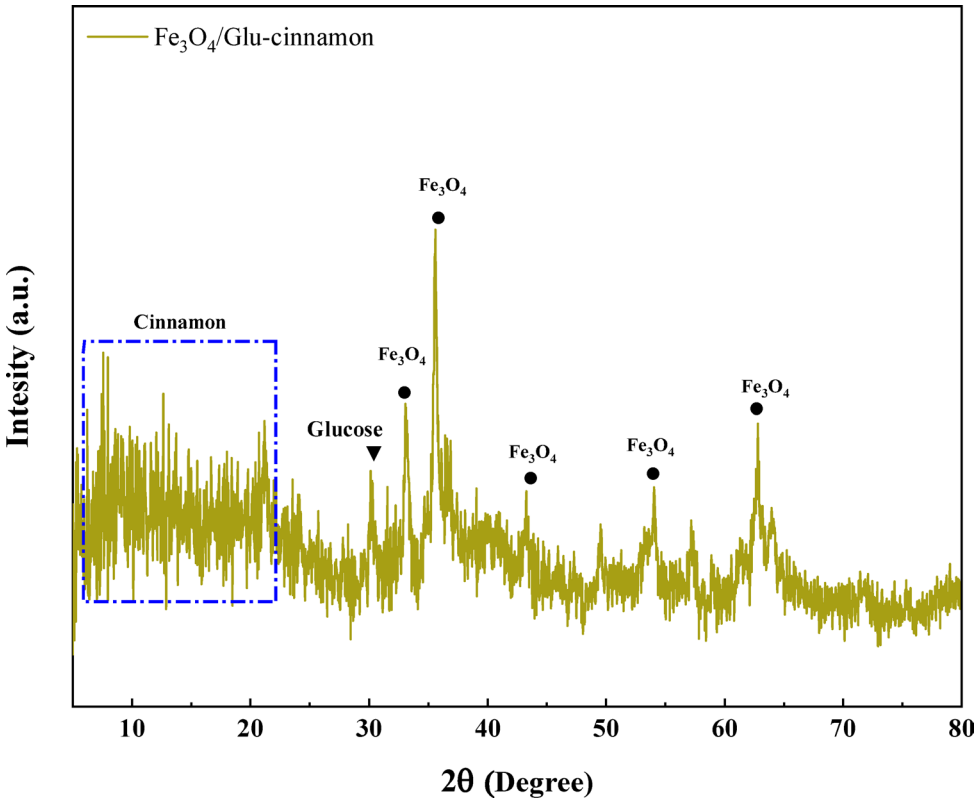

Fig. 8. XRD spectrum of Fe_3O_4@Glu-Cinnamon NPs.

of NPs[27]. The Fe_3O_4@Glu-Cinnamon NPs synthesized in this work exhibited similar physicochemical features to those synthesized in previous studies. Esfahani et al.[18] synthesized Fe_3O_4@Glu-Cinnamon NPs and reported that the NPs were spherical, with a size range of 20–60 nm, and without impurities. In addition, the DLS size and zeta potential of the particles were 190 nm and − 14.1 mV, respectively, which were similar to our work.

Cell viability assay indicated that Fe_3O_4@Glu-Cinnamon NPs were considerably more toxic to cancer cells than normal human cells. This observation is an important criterion in selecting potent anticancer agents. The higher susceptibility of cancer cells to the NPs may contribute to the functionalization of iron oxide NPs with glucose. Glucose is the main carbon source for human cells, which is used in various anabolic and catabolic pathways in human cells. Therefore, sufficient glucose uptake is crucial to guarantee normal metabolism and cell proliferation. Cancer cells have generally higher metabolic and proliferation rates than normal cells. It was found that high glucose levels can promote migration and invasion of colon cancer cells[28]. For this reason, cancer cells need to absorb larger amounts of nutrients from the surrounding environment to produce enough energy for their metabolic activities and create the precursors required for cell proliferation[29]. It seems that Fe_3O_4@Glu-Cinnamon NPs would have a higher uptake into the cancer cells than normal cells due to the functionalization with glucose, which leads to more efficient cytotoxic effects of the nanoparticles in cancer cells. The inhibitory effects of Fe_3O_4@Glu-Cinnamon NPs on cancer cells mainly contribute to the cytotoxic action of cinnamon. It has been reported that cinnamaldehyde-rich cinnamon induces cell death in colon cancer cell lines[11]. The IC_{50} value of cinnamon alone on the cancer cell line was higher compared to the Fe_3O_4@Glu-Cinnamon NPs. It seems that the reason for this higher level is that the NP penetrates the cell more easily, but cinnamon cannot enter the cell easily. In agreement with previous studies, we found that cinnamon has dose-dependent toxicity in the cancer cell line SW480. The cytotoxic properties of cinnamon contribute to its cinnamaldehyde contents. Several mechanisms have been proposed for the cytotoxic effects of cinnamaldehyde. It was reported that cinnamaldehyde can significantly inhibit the proliferation of breast cancer cells and induce apoptosis through the peroxisome proliferator-activated receptor and PI3K-Akt pathway[30]. Additionally, it was found that cinnamaldehyde can trigger intrinsic apoptosis in the leukemia cell line through the generation of reactive oxygen species (ROS)[31].

Flow cytometry analysis revealed that exposure to Fe_3O_4@Glu-Cinnamon NPs increased cell apoptosis in CRC cells. This finding was in agreement with previous studies, which reported cinnamaldehyde can trigger apoptotic pathways in various CRC cell lines such as SW480, HT-29 and HCT[32,33]. Reports are available about the induction of the intrinsic apoptosis in cancer cells by cinnamaldehyde, which are in agreement with our report[30]. Furthermore, we found that treated cells underwent nuclear alterations such as fragmented and condensed nuclei which are typical nuclear morphological changes that are observed in apoptotic cells. Similar apoptotic changes due to the treatment of CRC cells with cinnamaldehyde were observed by Li et al.[32] which is

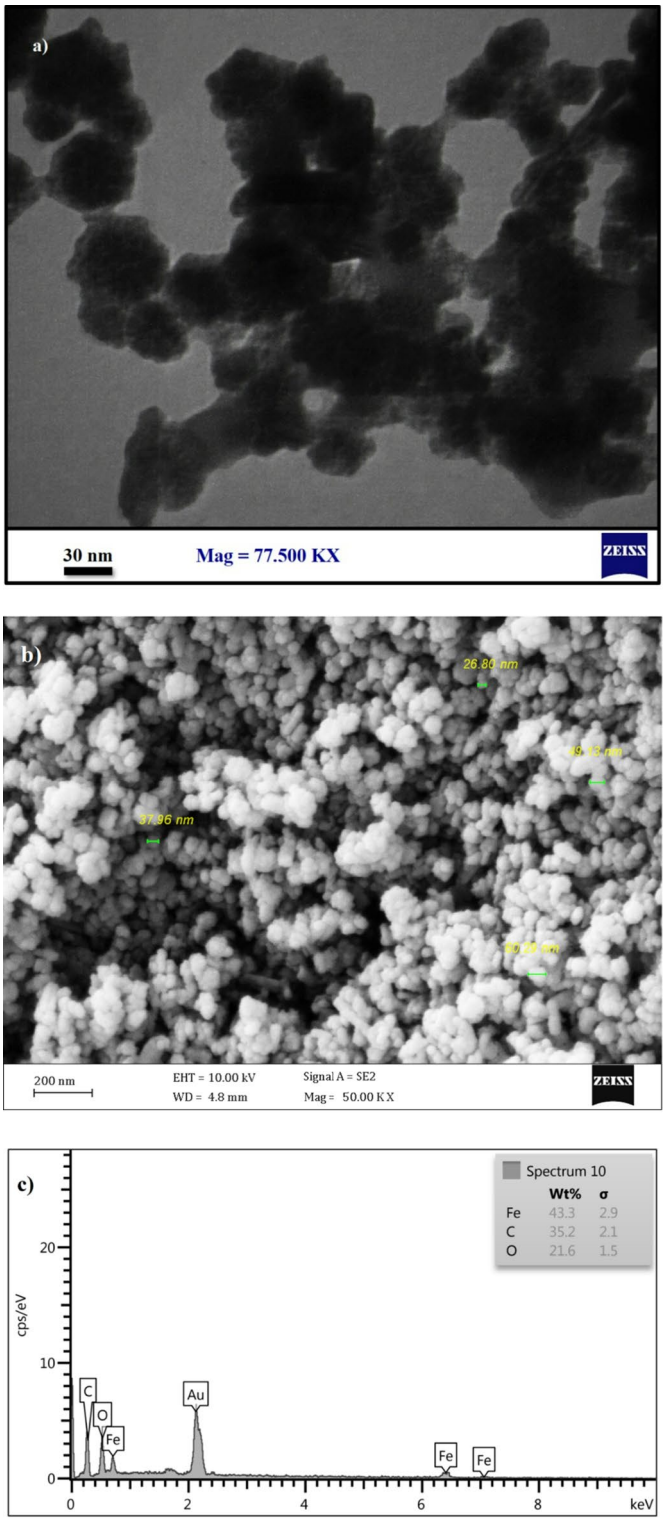

Fig. 9. (**a**) TEM and (**b**) SEM images and (**c**) EDS-mapping analysis of Fe_3O_4@Glu-Cinnamon NPs. The NPs contained no elemental impurity and were in a size range of 26.8–60.2 nm.

in agreement with this study. Accordingly, the proapoptotic property of the synthesized NPs was found that is possibly associated with cinnamon.

We also found that treatment with Fe_3O_4@Glu-Cinnamon NPs dysregulates the cell cycle of the CRC cell line. Previous works showed that cinnamaldehyde causes tubulin aggregation and dysregulates cell cycle regulatory proteins cdk1 and cdc25C in CRC cells. Exposure to cinnamaldehyde can increase the phosphorylation of cdk1 and reduce cdc25 levels, which results in an increased level of deactivated phosphor-cdk1, resulting in cell cycle

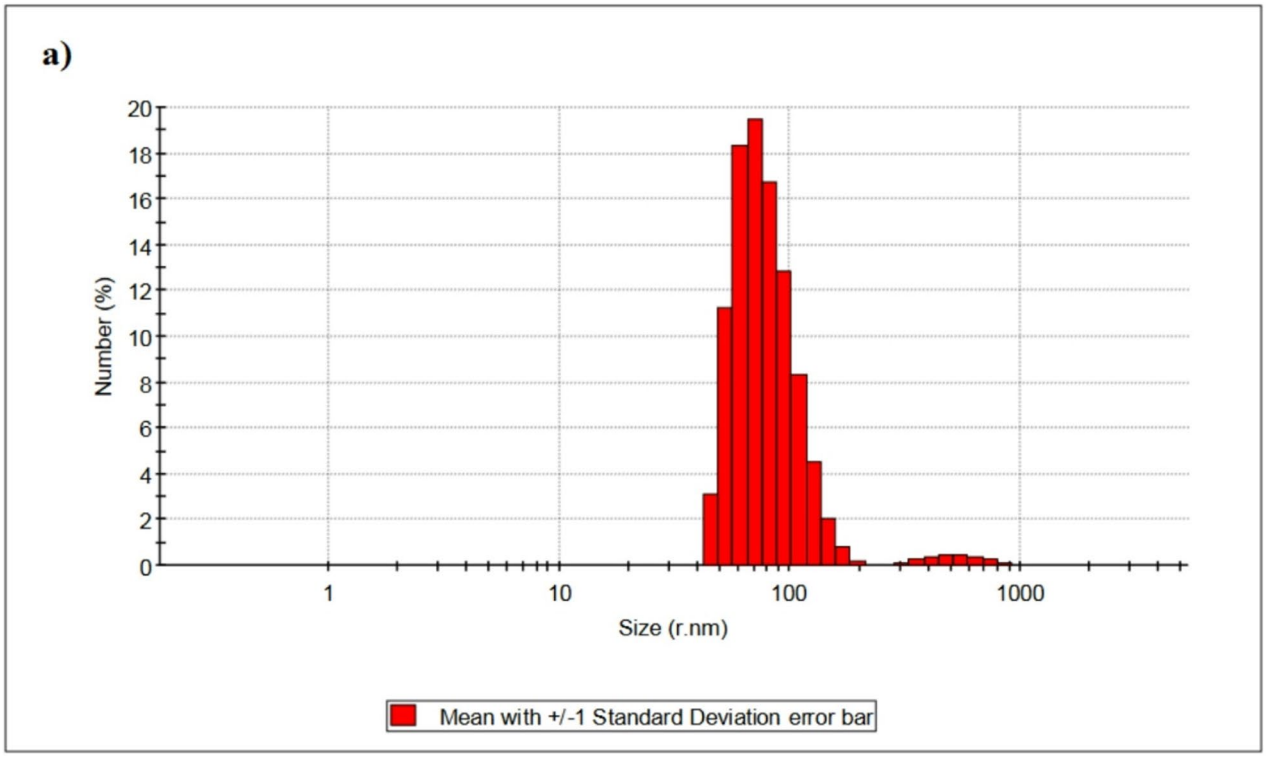

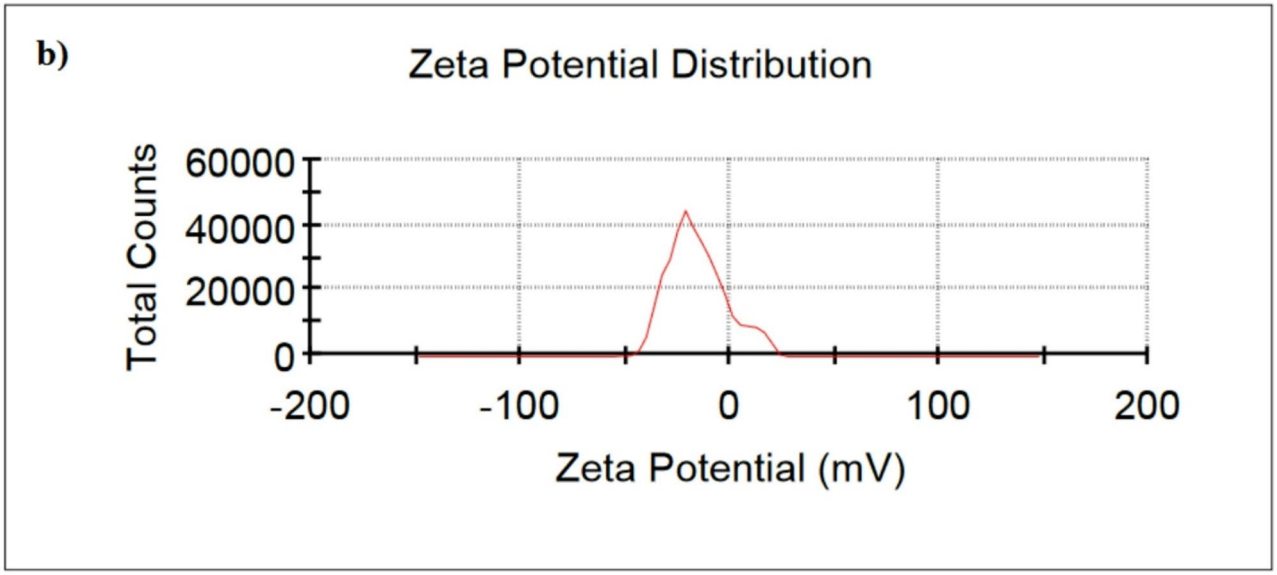

Fig. 10. (**a**) DLS and (**b**) zeta potential analyses of Fe_3O_4@Glu-Cinnamon NPs. The surface charge and zeta potential of the NPs were 213 nm and − 15.4 mV.

arrest, mainly at the G2 phase[34]. Additionally, the formation of cdk1/cyclin B1 complex is prohibited following exposure to cinnamaldehyde which would be likely a contributing cause of cell cycle arrest in the cells[34]. These events eventually cause cell cycle arrest in the treated cells and result in the initiation of apoptotic cell death.

Real-time PCR showed that treatment with Fe_3O_4@Glu-Cinnamon NPs causes downregulation of the SNAI1, THBS2 and INHBA oncogenes in the cancer cell line. The *SNAI1* gene encodes for a transcriptional factor SNAIL, which is typically overexpressed in fibroblast pathological conditions and contributes to the differentiation of epithelial cells to mesenchymal forms, which is associated to epithelial malignancy, invasion and metastasis[35,36]. Additionally, overexpression of SNAI1 is a contributing mediator of resistance to anticancer drugs such as oxaliplatin and cetuximab in patients with CRC[36]. Additionally, it was found that *SNAI1* is associated with the suppression of apoptosis and activation of the Wnt/β-catenin pathway that can promote the transformation of

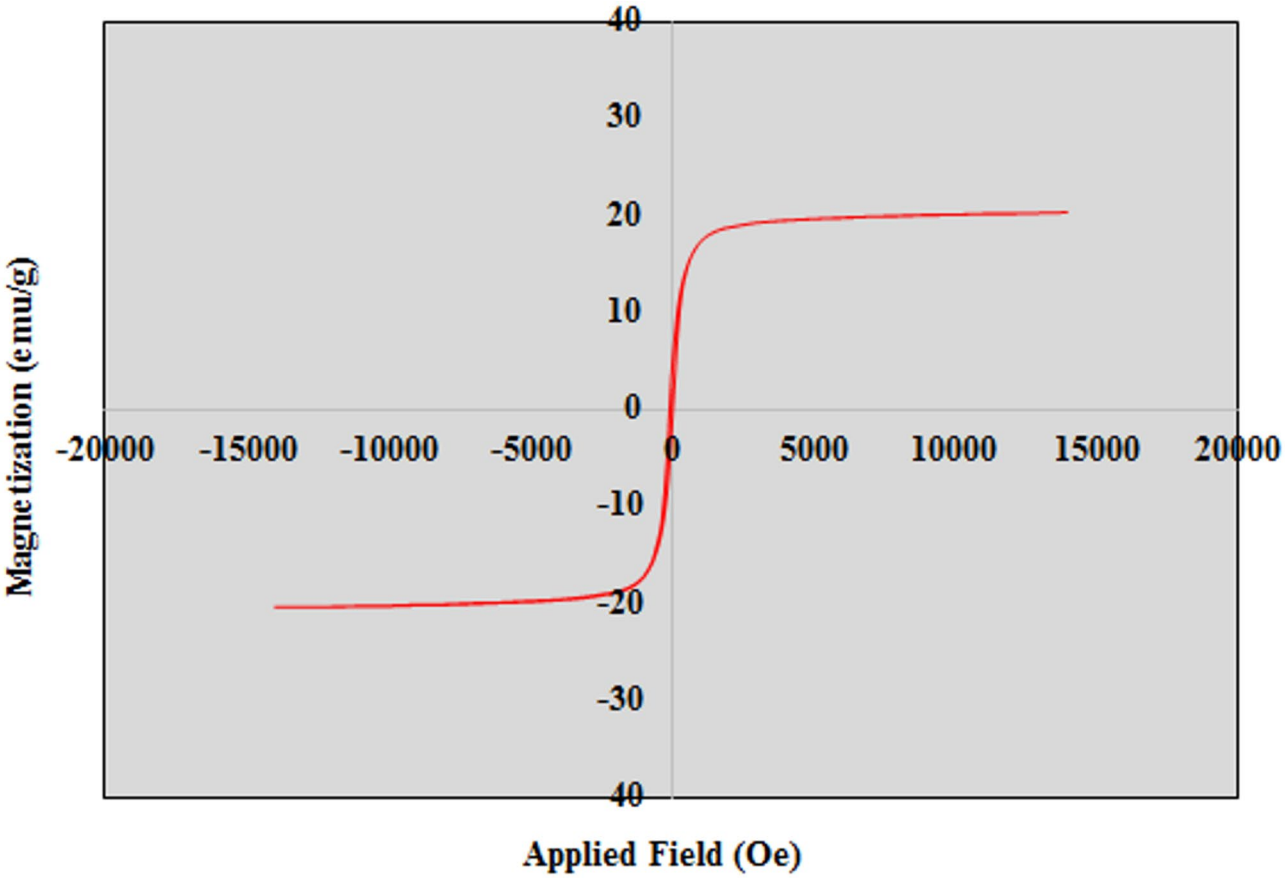

Fig. 11. Magnetization curve of Fe_3O_4@Glu-Cinnamon NPs. The maximum magnetization level of the NPs was 20.33 emu/g, which was observed at an applied field of 14,000 Oe.

colorectal fibroblasts and the development of colitis-associated CRC[37]. In normal cells, SNAI1 plays a key role in regulating epithelial-to-mesenchymal transition (EMT), contributing to cell migration, differentiation, and normal tissue development[38]. As observed in our study, the *SNAI1* is a candidate gene associated with mortality from CRC. The attenuation of this gene in the cancer cells that were treated with Fe_3O_4@Glu-Cinnamon NPs suggests the promising inhibitory effects of the NPs on CRC cells.

We found that treatment of the cancer cells with Fe_3O_4@Glu-Cinnamon NPs downregulated the *THBS2* expression to 0.66 folds which is a significant reduction in the transcript level of the gene. Thrombospondin-2 (THBS2) has various biological effects such as involvement in cell adhesion, motility as well as angiogenesis. It was found that *THBS2* has oncogenic effects, contributing to the invasiveness and development of several cancers. It was found that silencing of *THBS2* contributes to the inhibition of cell proliferation and invasion of cancer cells in CRC[38]. Wang et al.[39] reported that *THBS2* is highly expressed in CRC and associated with aggressiveness and migration of tumor cells through activation of the Wnt/β-catenin pathway. In normal cells, THBS2 is involved in extracellular matrix remodeling and plays a role in maintaining tissue homeostasis, regulating cell adhesion, and tissue repair. Inhibin βA (INHBA) is a member of the TGF-β superfamily which is associated with cell growth and differentiation through activation of the Smad2/Smad3 signaling pathway. An association between the overexpression of the *INHBA* gene and the development of various cancers, including CRC, has been reported[40]. It was found that silencing of *INHBA* inhibits the activation of TGF-β that leads to inhibition of cell proliferation, migration and invasiveness[41,42]. Therefore, this oncogene plays a crucial role in the development and severity of CRC. INHBA regulates cellular growth and differentiation through TGF-β signaling pathways, contributing to normal tissue homeostasis and repair[43]. The reduced expression of the *SNAI1*, *INHBA* and *THBS2* oncogenes suggest that Fe_3O_4@Glu-Cinnamon NPs can interfere with several signaling pathways in the CRC cell line, which reduce cell proliferation and invasiveness, and induce cell death through activation of apoptotic pathways. Since these oncogenes strongly influence the invasion and aggressiveness of CRC and contribute to mortality from this disease, this study provides promising results in the treatment of CRC using Fe_3O_4@Glu-Cinnamon NPs. Although the laboratory study was limited to genes associated with poor prognosis, bioinformatics analyses also considered genes linked to good prognosis, such as ACO1, ACO2, ACSD2, and PPARGC1A. These genes play essential roles in maintaining cellular homeostasis and metabolic processes. ACO1 and ACO2 are involved in mitochondrial function and energy production, contributing to the overall metabolic balance in normal cells[44]. ACSD2 regulates fatty acid metabolism and membrane integrity, which are crucial for maintaining cellular structure and function. Additionally, PPARGC1A is a key regulator of

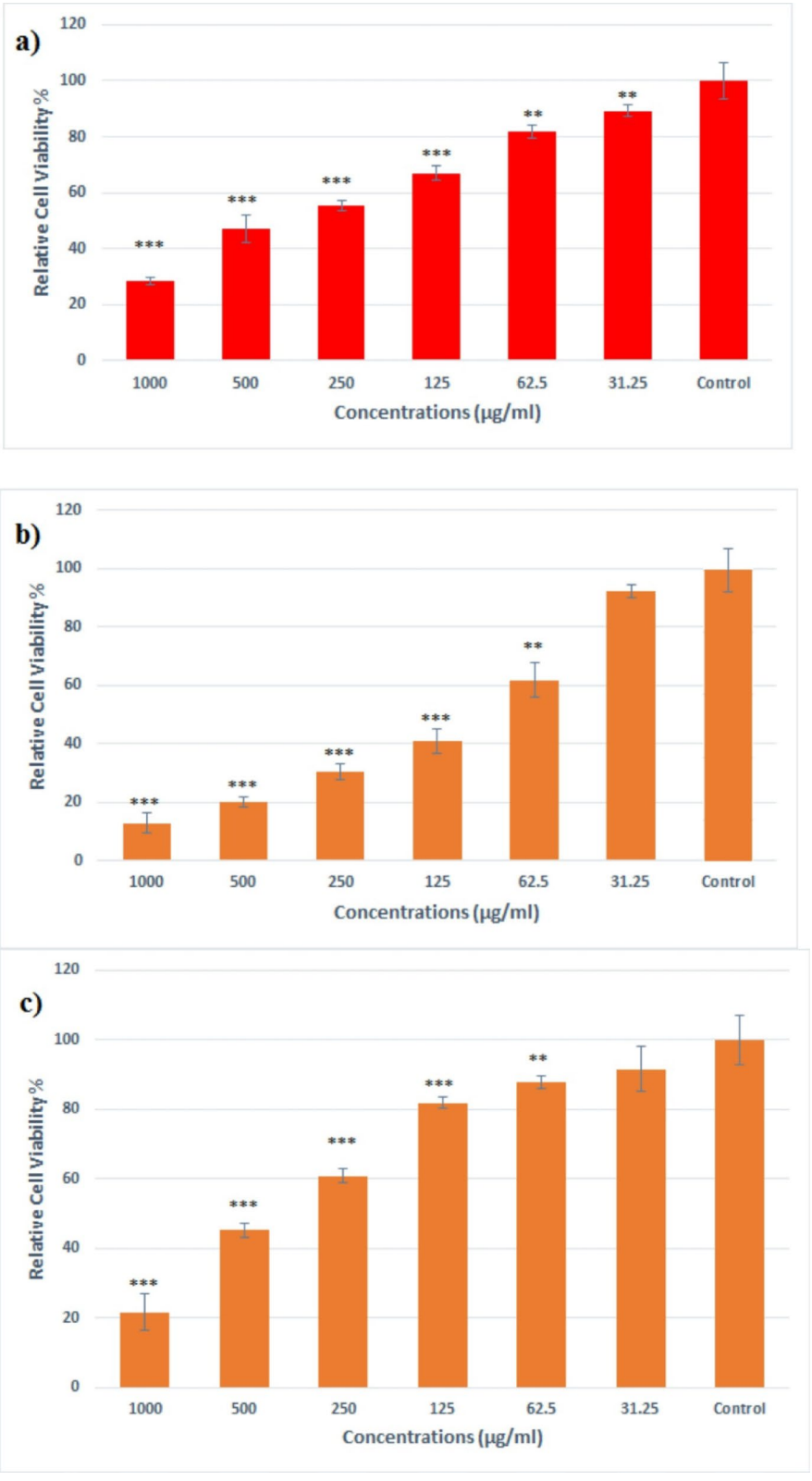

Fig. 12. Cell viability assay. Viability percentage of the normal (**a**) and CRC (**b**) cell lines treated with different concentrations of Fe_3O_4@Glu-Cinnamon NPs. (**c**) Viability of CRC cells treated with different concentrations of cinnamon. The IC_{50} value of Fe_3O_4@Glu-Cinnamon NPs for normal and CRC cells were 340 and 127 µg/mL, respectively and IC_{50} value of cinnamon alone for CRC cells was 362 µg/mL.

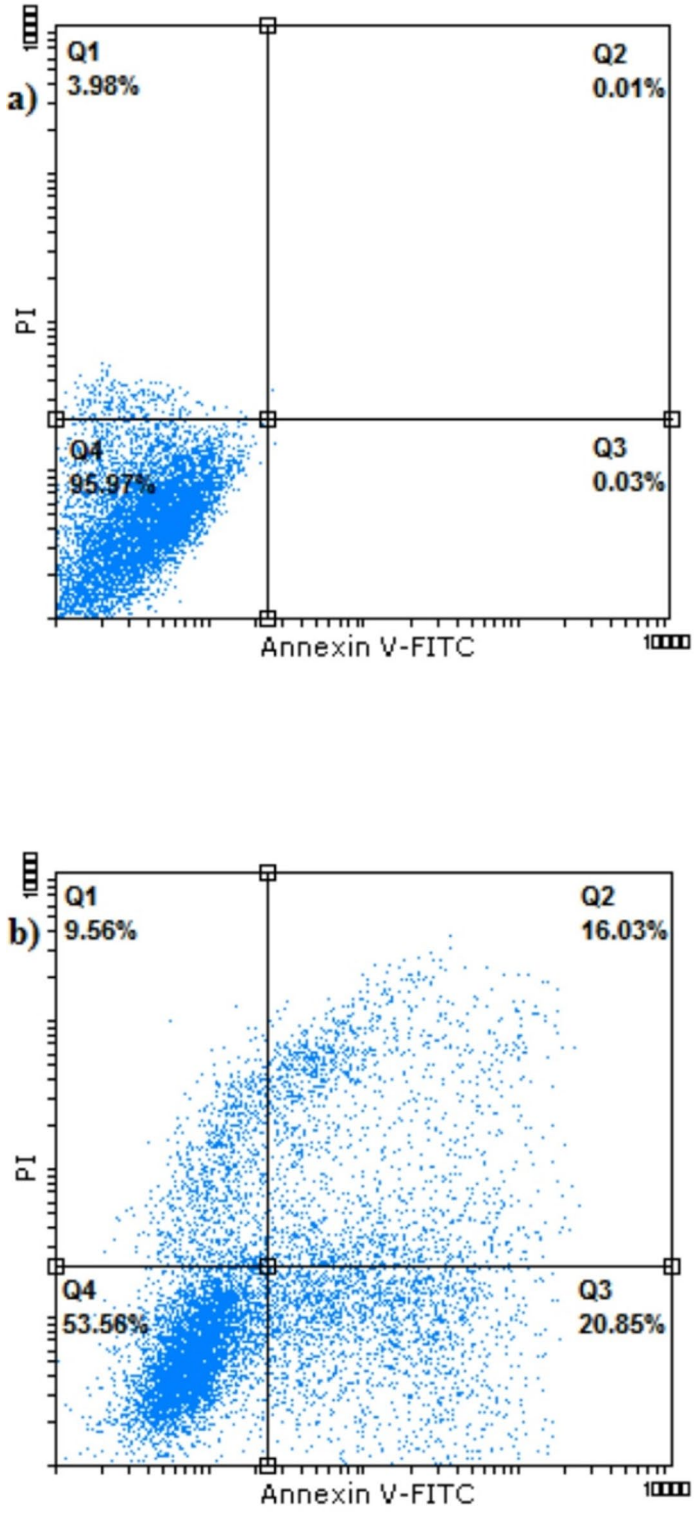

Fig. 13. Flow cytometry analysis of CRC cells. (**a**) control, (**b**) Treated with Fe_3O_4@Glu-Cinnamon NPs. Exposure to the NPs elevated primary and late apoptosis and cell necrosis levels. Q1; healthy cells, Q2: cell necrosis, Q3; late apoptosis and Q4; primary apoptosis.

mitochondrial biogenesis and oxidative stress response, supporting energy production and cellular adaptation to stress[45]. Future studies could explore these genes in greater detail to better understand their role in colorectal cancer progression and their potential therapeutic applications. Moreover, to confirm the therapeutic potential of Fe_3O_4@Glu-Cinnamon, future studies should evaluate their efficacy in colorectal cancer animal models.

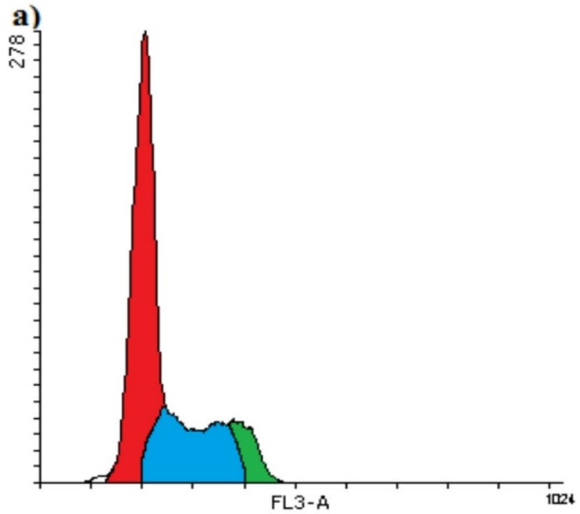

	Events	% of Vis	Mean	GeoMean	Median	CV
All events	10313	100	245.7404	236.0785	215	30.22414
SubG1	105	1.018132	125.2286	124.2869	127	12.0558
G0/G1	6475	62.78483	200.0956	199.3563	202	8.445824
S	2259	21.90439	285.5175	283.1774	282	12.83734
G2/M	1469	14.24416	393.4997	392.6562	391	6.581139

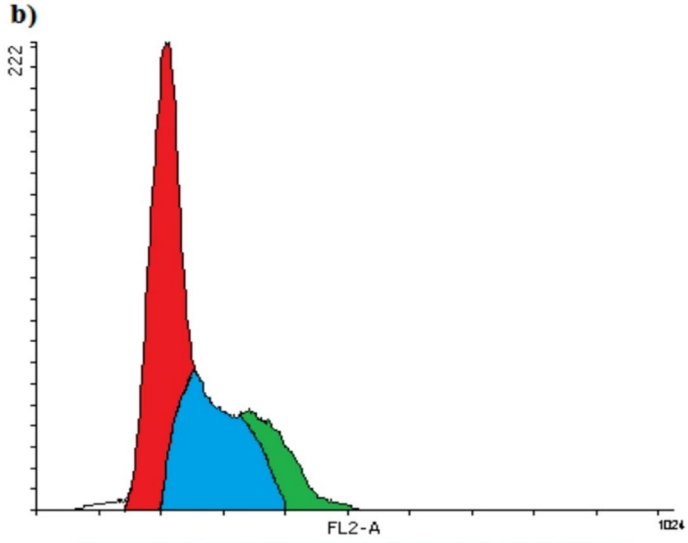

	Events	% of Vis	Mean	GeoMean	Median	CV
All events	10540	100	255.1525	245.2333	226	29.32186
SubG1	138	1.309298	116.8333	114.4352	120	19.44839
G0/G1	5305	50.33207	201.3533	200.6354	203	8.314996
S	3381	32.0778	276.2203	274.0595	271	12.62337
G2/M	1705	16.17647	390.3267	388.9075	383	8.707799

Fig. 14. Cell cycle analysis of CRC cells. (**a**) control, (**b**) Treated with Fe_3O_4@Glu-Cinnamon NPs. Exposure to the NPs caused cell cycle arrest mainly at the S and G2/M phases.

While our study demonstrates the downregulation of oncogenes (*SNAI1*, *THBS2*, and *INHBA*) and the induction of apoptosis, the exact molecular pathways underlying these effects remain to be fully elucidated. Future studies will focus on in-depth mechanistic analyses, including signaling pathway investigations and transcriptomic/proteomic profiling to determine the precise molecular interactions of Fe_3O_4@Glu-Cinnamon NPs with CRC cells. This was the limitation of our manuscript.

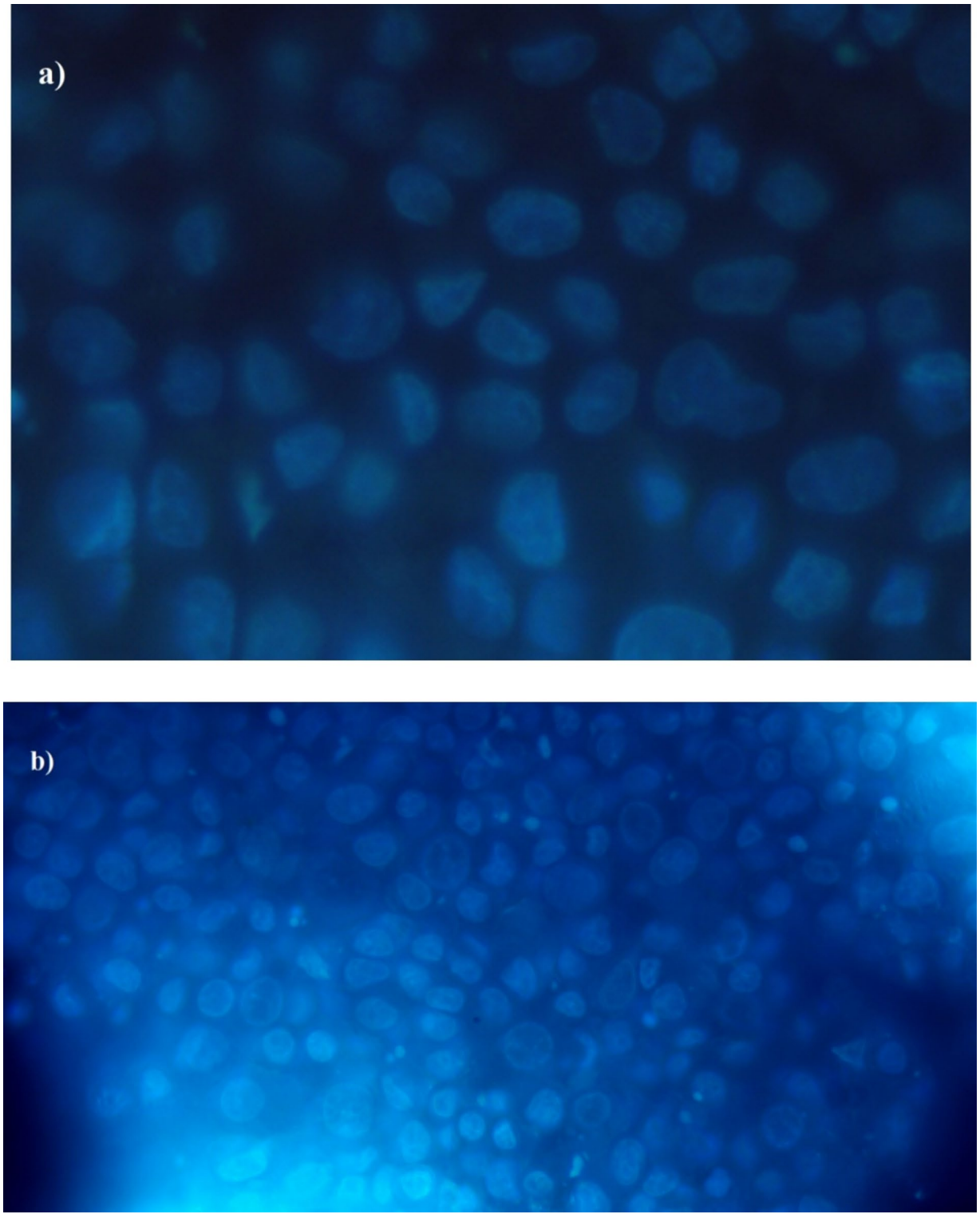

Fig. 15. Hoechst staining of CRC cells. (**a**) control, (**b**) Treated with Fe_3O_4@Glu-Cinnamon NPs. Exposure to the NPs caused nuclear alterations such as chromatin condensation and fragmentation.

Conclusion

In this study, the candidate oncogenes associated with the mortality of CRC were identified and the effect of Fe_3O_4@Glu-Cinnamon NPs on the survival of CRC cells (SW480) and the expression of these oncogenes was investigated. We found that the synthesized NPs reduced the viability of the CRC cells more efficiently than normal cells, and induced cell apoptosis/necrosis and cell cycle arrest at the S and G2/M phases in the CRC cells. In addition, the exposure to the NPs significantly reduced the expression of the mortality-associated oncogenes,

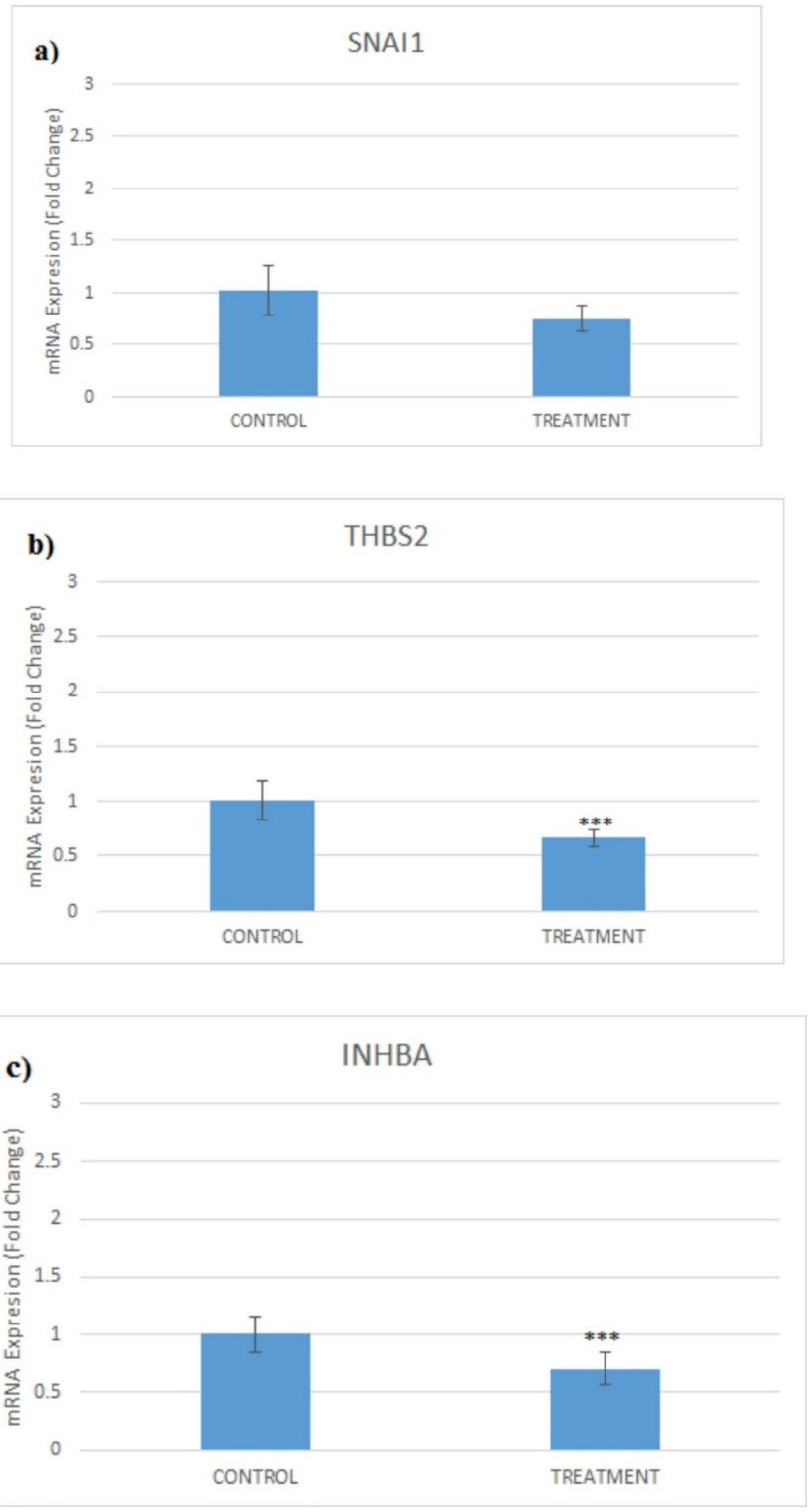

Fig. 16. The mRNA expression levels of the *SNAI1*, *THBS* and *INHBA* oncogenes in the CRC cells treated with Fe_3O_4@Glu-Cinnamon NPs relative to control cells. Exposure to the NPs reduced the mRNA levels of all oncogenes.

SNAI1, *THBS2* and *INHBA*. Fe_3O_4@Glu-Cinnamon NPs showed potent anticancer activity against CRC cells through apoptosis induction and attenuation of mortality-associated genes. The targeted delivery of cinnamon using the glucose-functionalized Fe_3O_4 NPs provides an innovative approach for the treatment of CRC, however, further research considering the toxicity effects and stability at in-vitro conditions is essential. Conjugation of

cinnamon to Fe_3O_4@Glu NPs can be considered for the development of safer therapeutics, aiming to explore these nanoparticles' efficacy in preclinical models, paving the way for eventual clinical trials.

Data availability

Data is provided within the manuscript.

Received: 11 December 2024; Accepted: 12 May 2025
Published online: 20 May 2025

References

1. Sung, H. et al. Global cancer statistics 2020: GLOBOCAN estimates of incidence and mortality worldwide for 36 cancers in 185 countries. *Cancer J. Clin.* **71** (3), 209–249. https://doi.org/10.3322/caac.21660 (2021).
2. Favoriti, P. et al. Worldwide burden of colorectal cancer: a review. *Updates Surg.* **68**, 7–11. https://doi.org/10.1007/s13304-016-0359-y (2016).
3. Tariq, K. & Ghias, K. Colorectal cancer carcinogenesis: a review of mechanisms. *Cancer Biology Med.* **13** (1), 120. https://doi.org/10.28092/j.issn.2095-3941.2015.0103 (2016).
4. Hu, J. et al. Magnetically active Fe 3 O 4 nanorods loaded with tissue plasminogen activator for enhanced thrombolysis. *Nano Res.* **9**, 2652–2661. https://doi.org/10.1007/s12274-016-1152-4 (2016).
5. Dhandapani, S. et al. Coprisin/Compound K conjugated gold nanoparticles induced cell death through apoptosis and ferroptosis pathway in adenocarcinoma gastric cells. *ACS Omega*. **9** (24), 25932–25944. https://doi.org/10.1021/acsomega.4c00554 (2024).
6. Elumalai, K., Srinivasan, S. & Shanmugam, A. Review of the efficacy of nanoparticle-based drug delivery systems for cancer treatment. *Biomedical Technol.* **5**, 109–122. https://doi.org/10.1016/j.bmt.2023.09.001 (2024).
7. Rezaei, B. et al. Magnetic nanoparticles: a review on synthesis, characterization, functionalization, and biomedical applications. *Small* **20** (5), 2304848. https://doi.org/10.1002/smll.202304848 (2024).
8. Peréz, D. L. et al. Synthesis of superparamagnetic iron oxide nanoparticles coated with polyethylene glycol as potential drug carriers for cancer treatment. *J. Nanopart. Res.* **26** (1), 2. https://doi.org/10.1007/s11051-023-05900-5 (2024).
9. Rajkumar, S. & Prabaharan, M. Multi-functional nanocarriers based on iron oxide nanoparticles conjugated with doxorubicin, Poly (ethylene glycol) and folic acid as theranostics for cancer therapy. *Colloids Surf., B.* **170**, 529–537. https://doi.org/10.1016/j.colsurfb.2018.06.051 (2018).
10. Wang, R. et al. 8-paradol from ginger exacerbates PINK1/Parkin mediated mitophagy to induce apoptosis in human gastric adenocarcinoma. *Pharmacol. Res.* **187**, 106610 (2023).
11. Nile, A. et al. Cinnamaldehyde-Rich cinnamon extract induces cell death in Colon cancer cell lines HCT 116 and HT-29. *Int. J. Mol. Sci.* **24** (9), 8191. https://doi.org/10.3390/ijms24098191 (2023).
12. Jaganathan, S. K. & Supriyanto, E. Antiproliferative and molecular mechanism of eugenol-induced apoptosis in cancer cells. *Molecules* **17** (6), 6290–6304. https://doi.org/10.3390/molecules17066290 (2012).
13. Muhoza, B. et al. Encapsulation of cinnamaldehyde: an insight on delivery systems and food applications. *Crit. Rev. Food Sci. Nutr.* **63** (15), 2521–2543. https://doi.org/10.1080/10408398.2021.1977236 (2023).
14. Nowak-Jary, J. & Machnicka, B. Pharmacokinetics of magnetic iron oxide nanoparticles for medical applications. *J. Nanobiotechnol.* **20** (1), 305. https://doi.org/10.1186/s12951-022-01510-w (2022).
15. Kumar, P., Singh, R. & Kush, P. Biocompatibility, toxicity concerns, environmental and safety considerations, and legal aspects of functionalized magnetic nanoparticles. *Functionalized Magn. Nanopart. Theranostic Appl.* 533–558. https://doi.org/10.1002/9781394172917.ch17 (2024).
16. Wani, K. D. et al. Synthesis, characterization and in vitro study of biocompatible cinnamaldehyde functionalized magnetite nanoparticles (CPGF Nps) for hyperthermia and drug delivery applications in breast cancer. *PloS One*. **9** (9), e107315. https://doi.org/10.1371/journal.pone.0107315 (2014).
17. Mahdavi Niyaki, Z., Salehzadeh, A., Peymani, M. & Zaefizadeh, M. Exploring the therapeutic potential of Fe_3O_4@ glu-oleuropein nanoparticles in targeting KRAS pathway-regulating LncRNAs in colorectal cancer cells. *Biol. Trace Elem. Res.* **202** (7), 3073–3085. https://doi.org/10.1007/s12011-023-03892-w (2024).
18. Esfahani, M. A., Salehzadeh, A. & Ghobeh, M. Anti-Proliferative Activity of Magnetic Iron Oxide Nanoparticles Functionalized Glucose and Conjugated Cinnamon Against Gastric Cell Line. *BioNanoScience*, 1–11. (2024). https://doi.org/10.1007/s12668-024-01562-2
19. Salehzadeh, A., Naeemi, A. S., Khaknezhad, L., Moradi-Shoeili, Z. & Shandiz, S. A. S. Fe_3O_4/Ag nanocomposite biosynthesized using *Spirulina platensis* extract and its enhanced anticancer efficiency. *IET Nanobiotechnology*. (2019). https://doi.org/10.1049/iet-nbt.2018.5364.
20. Narayani, S. S., Saravanan, S., Ravindran, J., Ramasamy, M. S. & Chitra, J. In vitro anticancer activity of fucoidan extracted from Sargassum cinereum against Caco-2 cells. *Int. J. Biol. Macromol.* **138**, 618–628. https://doi.org/10.1016/j.ijbiomac.2019.07.127 (2019).
21. Pfaffl, M. W. A new mathematical model for relative quantification in real-time RT-PCR. *Nucleic Acids Res.* **29**, e45. https://doi.org/10.1093/nar/29.9.e45 (2001).
22. Emami, N., Farhadian, M., Solaimany Nazar, A. R. & Tangestaninejad, S. Adsorption of cefixime and lamotrigine on HKUST-1/ZIF-8 nanocomposite: isotherms, kinetics models and mechanism. *Int. J. Environ. Sci. Technol.* **20** (2), 1645–1672. https://doi.org/10.1007/s13762-022-04679-7 (2023).
23. Mikaeili Ghezeljeh, S., Salehzadeh, A. & Ataei-e Jaliseh, S. Iron oxide nanoparticles coated with glucose and conjugated with Safranal (Fe_3O_4@ Glu-Safranal NPs) inducing apoptosis in liver cancer cell line (HepG2). *BMC Chem.* **18** (1), 33. https://doi.org/10.1186/s13065-024-01142-1 (2024).
24. Dhanalakshmi, A. et al. Structural and optical characterization of ZnO and glucose capped ZnO nanoparticles. *Journal New. Mater. Electrochem. Systems*, **21**(1). (2018).
25. Xi, Y. & Xu, P. Global colorectal cancer burden in 2020 and projections to 2040. *Translational Oncol.* **14** (10), 101174. https://doi.org/10.1016/j.tranon.2021.101174 (2021).
26. Zhou, Z. & Li, M. Targeted therapies for cancer. *BMC Med.* **20** (1), 90. https://doi.org/10.1186/s12916-022-02287-3 (2022).
27. Jimenez-Ruiz, A., Perez-Tejeda, P., Grueso, E., Castillo, P. M. & Prado-Gotor, R. Nonfunctionalized gold nanoparticles: synthetic routes and synthesis condition dependence. *Chemistry–A Eur. J.* **21** (27), 9596–9609. https://doi.org/10.1002/chem.201405117 (2015).
28. Lin, C. Y. et al. Impact of high glucose on metastasis of colon cancer cells. *World J. Gastroenterology: WJG.* **21** (7), 2047. https://doi.org/10.3748/wjg.v21.i7.2047 (2015).
29. Papalazarou, V. & Maddocks, O. D. Supply and demand: cellular nutrient uptake and exchange in cancer. *Mol. Cell.* **81** (18), 3731–3748. https://doi.org/10.1016/j.molcel.2021.08.026 (2021).
30. Liu, Y. et al. Targets and mechanism used by cinnamaldehyde, the main active ingredient in cinnamon, in the treatment of breast cancer. *Front. Pharmacol.* **11**, 582719. https://doi.org/10.3389/fphar.2020.582719 (2020).

31. Ka, H. et al. Cinnamaldehyde induces apoptosis by ROS-mediated mitochondrial permeability transition in human promyelocytic leukemia HL-60 cells. *Cancer Lett.* **196** (2), 143–152. https://doi.org/10.1016/S0304-3835(03)00238-6 (2003).
32. Li, J., Teng, Y., Liu, S., Wang, Z., Chen, Y., Zhang, Y., … Zou, X. (2016). Cinnamaldehyde affects the biological behavior of human colorectal cancer cells and induces apoptosis via inhibition of the PI3K/Akt signaling pathway. Oncology reports, 35(3), 1501–1510. https://doi.org/10.3892/or.2015.4493.
33. Yu, C., Liu, S. L., Qi, M. H. & Zou, X. Cinnamaldehyde/chemotherapeutic agents interaction and drug-metabolizing genes in colorectal cancer. *Mol. Med. Rep.* **9** (2), 669–676. https://doi.org/10.3892/mmr.2013.1830 (2014).
34. Nagle, A. A. et al. Induction of tumor cell death through targeting tubulin and evoking dysregulation of cell cycle regulatory proteins by multifunctional cinnamaldehydes. *PloS One*. **7** (11), e50125. https://doi.org/10.1371/journal.pone.0050125 (2012).
35. Hoshino, H., Miyoshi, N., Nagai, K. I., Tomimaru, Y., Nagano, H., Sekimoto, M., …Ishii, H. (2009). Epithelial–mesenchymal transition with expression of SNAI1-induced chemoresistance in colorectal cancer. Biochemical and biophysical research communications, 390(3), 1061–1065. https://doi.org/10.1016/j.bbrc.2009.10.117.
36. Stanisavljevic, J., Loubat-Casanovas, J., Herrera, M., Luque, T., Pena, R., Lluch,A., … Baulida, J. (2015). Snail1-expressing fibroblasts in the tumor microenvironment display mechanical properties that support metastasis. Cancer research, 75(2), 284–295. https://doi.org/10.1158/0008-5472.CAN-14-1903.
37. Qing, F., Xue, J., Sui, L., Xiao, Q., Xie, T., Chen, Y., … Liu, Z. (2023). Intestinal epithelial SNAI1 promotes the occurrence of colorectal cancer by enhancing EMT and Wnt/β-catenin signaling. Medical Oncology, 41(1), 34. https://doi.org/10.1007/s12032-023-02253-w.
38. Batlle, E. & Massagué, J. Transforming growth factor-β signaling in immunity and cancer. *immuni*ty, 50(4), 924–940. https://doi.org/j.immuni.2019.03.024 (2019).
39. Wang, X. et al. THBS2 is a potential prognostic biomarker in colorectal cancer. *Sci. Rep.* **6** (1), 33366. https://doi.org/10.1038/srep33366 (2016).
40. Dean, M., Davis, D. A. & Burdette, J. E. Activin A stimulates migration of the fallopian tube epithelium, an origin of high-grade serous ovarian cancer, through non-canonical signaling. *Cancer Lett.* **391**, 114–124. https://doi.org/10.1016/j.canlet.2017.01.011 (2017).
41. Chen, Z. L., Qin, L., Peng, X. B., Hu, Y. & Liu, B. INHBA gene Silencing inhibits gastric cancer cell migration and invasion by impeding activation of the TGF-β signaling pathway. *J. Cell. Physiol.* **234** (10), 18065–18074. https://doi.org/10.1002/jcp.28439 (2019).
42. He, Z., Liang, J. & Wang, B. Inhibin, beta A regulates the transforming growth factor-beta pathway to promote malignant biological behaviour in colorectal cancer. *Cell Biochem. Funct.* **39** (2), 258–266. https://doi.org/10.1002/cbf.3573 (2021).
43. Xueqin, T., Jinhong, M. & Yuping, H. Inhibin subunit beta A promotes cell proliferation and metastasis of breast cancer through Wnt/β-catenin signaling pathway. *Bioengineered* **12** (2), 11567–11575. https://doi.org/10.1080/21655979.2021.1971028 (2021).
44. Padalko, V., Posnik, F. & Adamczyk, M. Mitochondrial aconitase and its contribution to the pathogenesis of neurodegenerative diseases. *Int. J. Mol. Sci.* **25** (18), 9950. https://doi.org/10.3390/ijms25189950 (2024).
45. ZadeganFG. et al. Cardiac differentiation of mouse embryonic stem cells is influenced by a PPAR γ/PGC-1α-FNDC5 pathway during the stage of cardiac precursor cell formation. *Eur. J. Cell Biol.* **257**, 66. https://doi.org/10.1016/j.ejcb.2015.04.002 (2015).

Author contributions

A.S. and M.P.: Conceptualization. A.S. and M.P.: Methodology. A.S. and M.P.: Formal analysis and investigation. A.S., M.A.A.CH. and M.P.: Writing Original Draft Preparation. M.A.A.CH.: Resources. A.S. and M.P.: Supervision.

Funding

This research received no specific grant from any funding agency in the public, commercial, or not-for-profit sectors.

Declarations

Competing interests

The authors declare no competing interests.

Additional information

Supplementary Information The online version contains supplementary material available at https://doi.org/10.1038/s41598-025-02189-3.

Correspondence and requests for materials should be addressed to A.S.

Reprints and permissions information is available at www.nature.com/reprints.

Publisher's note Springer Nature remains neutral with regard to jurisdictional claims in published maps and institutional affiliations.